TRIBHUVAN UNIVERSITY

INSTITUTE OF ENGINEERING

PULCHOWK CAMPUS

Thesis No.: M-337-MSREE-2018-2022

Enhancing the Transient Stability of PV-Hydro Microgrid using Virtual Synchronous Machine (VSM)

by

Sanjeev Kumar Sah

A THESIS

SUBMITTED TO THE DEPARTMENT OF MECHANICAL AND AEROSPACE ENGINEERING

IN PARTIAL FULFILLMENT OF THE REQUIREMENTS

FOR THE DEGREE OF MASTER OF SCIENCE IN

RENEWABLE ENERGY ENGINEERING

DEPARTMENT OF MECHANICAL AND AEROSPACE ENGINEERING

LALITPUR, NEPAL

MARCH, 2022

COPYRIGHT

TRIBHUWAN UNIVERSITY

INSTITUTE OF ENGINEERING

PULCHOWK CAMPUS

DEPARTMENT OF MECHANICAL AND AEROSPACE ENGINEERING

The undersigned certify that they have read, and recommended to the Institute of Engineering for acceptance, a thesis entitled **"Enhancing the Transient Stability of PV-Hydro Microgrid using Virtual Synchronous Machine (VSM)"** submitted by Sanjeev Kumar Sah in partial fulfillment of the requirements for the degree of Master of Science in Renewable Energy Engineering.

_____

Supervisor, Dr. Shree Raj Shakya

Associate Professor

Department of Mechanical and Aerospace Engineering

_____

External Examiner, Dr. Shailendra Kumar Jha

Associate Professor

Kathmandu University

_____

Committee Chairperson, Dr. Surya Prasad Adhikari

Head of Department

Department of Mechanical and Aerospace Engineering

March 21, 2022

Date

ABSTRACT

Renewable energy sources such as solar, wind, and biomass are being integrated into electrical networks in order to meet demand while reducing dependency on non-renewable
sources such as petroleum products, coal, and natural gas are attracting a great deal of attention. The bulk of distributed generators (DGs) are linked to the utility grid through power electronics-based converters, which have either extremely little or no spinning mass
and damping property, reducing total system inertia and transient stability. It would cause a significant change in the frequency of the system if large load changes in the system. This may be improved by using a Virtual Synchronous Machine (VSM) to simulate the inertial and damping properties of a real generator. A VSM is a power electronics device that stores short-term energy and has a dispatching mechanism that allows it to operate like a synchronous generator. VSM simulates the inertial and damping qualities of a synchronous machine, and it may either inject or absorb power into or from the grid in a manner similar to the injection or absorption of kinetic energy in synchronous generators. This study investigates the possibility of using VSM to increase grid stability under transient conditions. Unlike many previous efforts, this study proposes a way of regulating VSM operation utilizing power angle control. An angle controller is built using a small signal model of the swing equation that is linearized round the operating point. The suggested power angle control method has been implemented in the VSM and the system was simulated in MATLAB/Simulink. A system under this study considers the hydro of 150kVA capacity which has been connected with the PV of 10 kW. The substantial load is switched on so that the frequency deviation increases beyond the normal range. The transient stability was then improved by implementing the VSM by improving the frequency deviation from 19% to 7%.

ACKNOWLEDGEMENTS

The successful completion of this thesis work would not have been possible without the guidance and support of many people and I am extremely grateful to all of them. I would like to offer my thankfulness to my thesis supervisor Associate Professor Dr. Shree Raj Shakya for his invaluable guidance, support, and encouragement throughout this thesis work.

I would like to express my sincere appreciation to all teachers and staffs of the Department of Mechanical and Aerospace Engineering, Pulchowk Campus for their continuous support and guidance.

I would like to thank my parents for their unconditional love and support. I must thank my wonderful wife, Dr. Swati Shah, as without her mental, motivational support, I may never have completed this thesis. I would also like to give special thanks to my son Poman Pratap Shah for his understanding, and patience. I also thank my daughter Samira Shah for being such a patient with a smiling attitude.

Last but not the least, I would like to acknowledge all people who have contributed directly or indirectly to complete this thesis work.

TABLE OF CONTENTS

LIST OF FIGURES

LIST OF ABBREVIATIONS

AC	:	Alternating Current
CT	:	Current Transformer
DC	:	Direct Current
DES	:	Distributed Energy Sources
IEEE	:	Institute of Electrical and Electronics Engineer
MATLAB	:	Matrix Laboratory
Op-Amp	:	Operational Amplifier
PLL	:	Phase Locked Loop
PU	:	Per Unit
PV	:	Photovoltaic
RES	:	Renewable Energy Sources
ROCOF	:	Rate of Change of Frequency
VSI	:	Voltage Source Inverter
VSM	:	Virtual Synchronous Machine

CHAPTER ONE: INTRODUCTION

1.1 Background

Renewable energy sources such as solar, wind, and biomass are being integrated into electrical networks in order to meet demand while reducing dependency on non-renewable sources such as petroleum products, coal, and natural gas are attracting a great deal of attention (May *et al.*, 2015). The usage of distributed generators (DGs) as a more sophisticated application of renewable energy sources is becoming more popular. When it comes to rural areas with abundant hydropower resources and where the electric infrastructure has not yet been developed, Distributed Energy Sources (DES) such as Photovoltaic (PV)-hydro hybrid micro-grid systems are desirable (Fleissner *et al.*, 1974). However, as the penetration of these types of renewable energy sources increases, the overall inertia of the system reduces, which has a significant influence on the system's transient stability (Yan *et al.*, 2016). A major change in load in such systems may result in a big frequency disturbance, as well as a significant rate of change of frequency (ROCOF). As a result, in order to increase the stability of the system during the transient phase, greater inertia must be provided to the system. This can be done by using a Virtual Synchronous Machine (VSM) (Fleissner *et al.*, 1974; Cheema, 2020).

The function of VSM can be demonstrated in PV-hydro micro-grid whose overall inertia is low. As seen in Figure 1.2 (Adhikari *et al.*, 2018), the capacity of the system rises when PV is installed in contrast to the capacity of the system without PV. However, since PV generates zero inertia, the total inertia of the system has stayed constant. The transient stability of the system is significantly impacted as a result of this. Figure 1.3 (Adhikari *et al.*, 2018) shows an example of how VSM might be used to alleviate this issue. VSM helps to increase total inertia, allowing for greater transient stability.

Consider a micro-grid with only rotating generators:

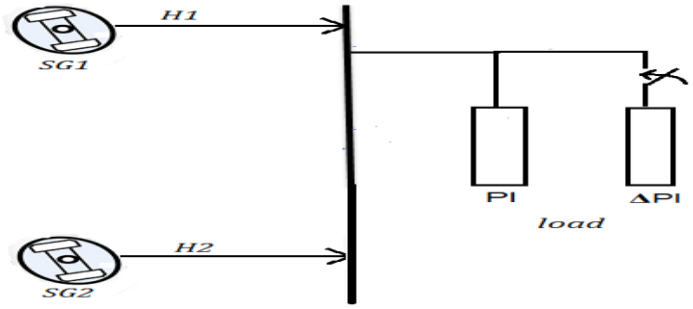

Figure 1.1 Micro-grid with only rotating generators (Adhikari et al., 2018)

Figure 1.1 shows the micro-grid with only the rotating generators. The overall inertia of parallel operations of two generators is the sum of individual inertias.

H_1 = Inertia of SG-1

H_2 = Inertia of SG-2

$H = H_1 + H_2$ Equation 1.1

Here, the overall inertia of the system is increased.

Consider a micro-grid including PV and Hydro system:

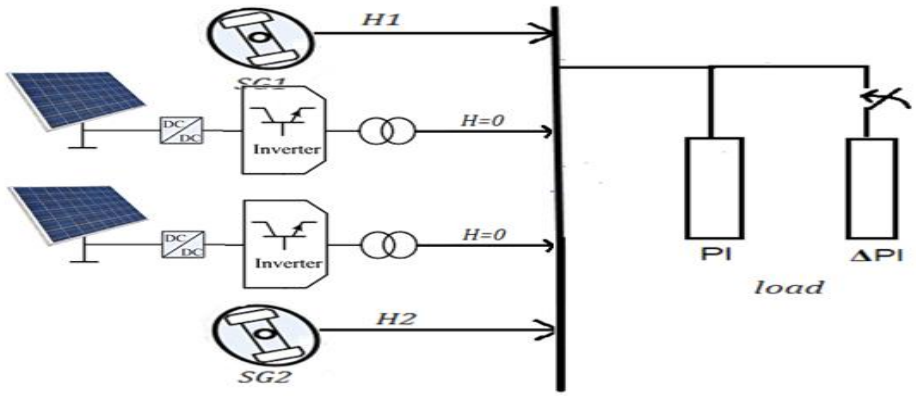

Figure 1.2 Integrated system containing micro-grid with PV-hydro system (Adhikari *et al.*, 2018)

In above PV-Hydro Micro-Grid, overall capacity of the plant has increased.

But, $H = H_1 + H_2$.

The overall inertia of the system has not increased. Hence, transient stability of PV-hydro micro-grid will be poor.

Micro-grid with VSM

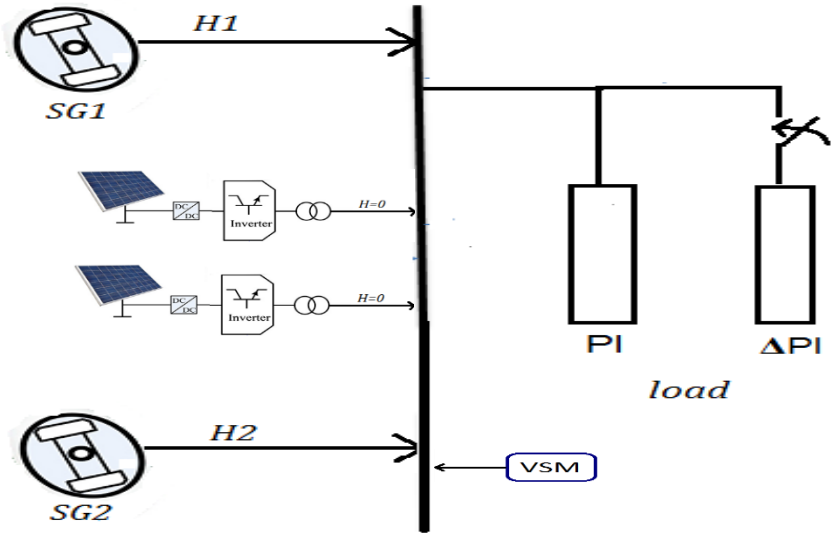

Figure 1.3 Micro-grid with VSM (Adhikari *et al.*, 2018)

In order to improve the transient stability of such integrated PV-hydro micro-grids, Virtual Synchronous Machines (VSM) can be used as shown in Figure 1.3.

1.2 Problem Statement

As the percentage of photovoltaics (PV) in PV-hydro integrated systems grows, the system's relative inertia reduces as a result of the absence of spinning masses, as in a typical synchronous generator (Fleissner *et al.*, 1974). A frequency instability issue arises, and this may have a major influence on the system's dynamic performance as well

as its transient stability (Song, Bi and Yang, 2005; Cheema, 2020). A number of strategies have been proposed to increase the transient performance of microgrids (Song, Bi and Yang, 2005; Adhikari *et al.*, 2018), all of which have been tested. System inertia may be artificially increased by using modified droop control methods, synchronverters, virtual synchronous generators (VSGs) or virtual synchronous machines (VSMs), and modified VSG control, all of which are available (Meng, Liu and Liu, 2019).

1.3 Research Objective

1.3.1 Main Objective

To design and simulate Virtual Synchronous Machine (VSM) for improving the transient stability of Microgrid during load perturbation by maintaining stable frequency through power absorption from or injection to the grid.

1.3.2 Specific Objectives

- To bring the transient condition in a system of 160 kVA capacity consisting of 150 kVA Hydro and 10 kW PV, where frequency deviates by greater than 15%, by switching load.
- To enhance the transient stability by keeping the frequency deviation within tolerable range thereby maintaining the stability using VSM.

CHAPTER TWO: LITERATURE REVIEW

2.1 Power System Stability

Power system stability refers to the capacity of an electric power system to re-establish its state of operational equilibrium after an interruption in service (Song, Bi and Yang, 2005). It is possible for a variety of disruptions to develop in a power system, including unanticipated increases in load demand, line-to-line faults, short circuits between transmission lines and the ground, and three-phase faults, among others (Phan *et al.*, 2019). We expect the electricity system to adjust to the new conditions and continue to function when there is only a little change or disturbance. However, although a significant disruption such as the sudden loss of a generator or the construction of a short circuit in the transmission system may not cause the afflicted region to be isolated from the rest of the grid, it may induce a fundamental change in the electrical power system (Song et al., 2005; Tamrakar et al., 2016; Zhong & Hornik, 2012). In power system studies, a range of stability categories are mentioned in order to establish the cause of the system's instability and to provide remedies to enhance the system's stability and reliability.

2.2 Synchronous Generator Operation

As shown in Figure 2.1 (Fitzgerald, Kingsley and Umans, 2003), The machine's field winding is wrapped around the rotor, while the armature windings are wrapped around the stator. Damped windings are also included in this design, and they are engaged when the machine is in a transitory condition of operation, and they aid to keep the machine functioning smoothly during that time.

There are two fundamental properties of a synchronous generator that have been identified as being very significant in the functioning of a power system that is steady and efficient. A synchronous generator's inherent properties (Fitzgerald, Kingsley and Umans, 2003; Ceraolo and Poli, 2014) include the following two features that are particularly noteworthy:

1. Inertia caused by the spinning masses
2. The damping effect produced by rotor's damper windings

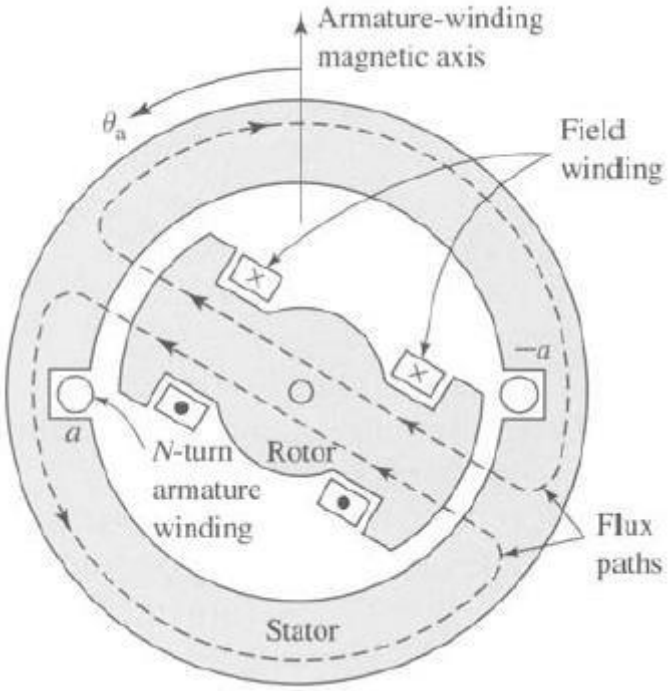

Figure 2.1 Schematic view of two pole synchronous generator

2.2.1 Inertia caused by the Spinning Masses

In the air gap, there is a sinusoidal rotating flux which is created by the synchronous generator's rotor in conjunction with the field and damper windings as it spins. This sinusoidal rotating flux finally results in an electromotive force at the armature terminals (Fitzgerald, Kingsley and Umans, 2003).

Taking a look at the swing equation (Fitzgerald, Kingsley and Umans, 2003) for synchronous generator dynamics, we can see that

$$Tm - Te = \frac{2Hd^2\delta}{w_o dt^2} + \frac{K_D}{w_o}\frac{d\delta}{dt} \qquad \text{Equation 2.1}$$

Where; H= per unit inertia constant

Tm=mechanical torque in Nm

Te = electromagnetic torque in Nm

W_0= angular velocity of the rotor, mech. rad/s

K_D= Damping coefficient in pu torque/pu speed deviation

δ= angular position of the rotor in electrical rad/s

The pace at which the rotor's speed changes is determined by the mass's inertia. Kinetic energy conserved in a spinning mass during steady operation may be particularly advantageous when there is an imbalance in torque. It will be absorbed by the system when there is an imbalance in the amount of kinetic energy available (Fitzgerald, Kingsley and Umans, 2003; Ceraolo and Poli, 2014).

2.2.2 Damping effect produced by Rotor's Damper Windings

When the generator rotor suffers rotor speed deviations owing to tiny disturbances, damper winding, which creates the damping effect, plays a crucial role in regaining synchronism (Fitzgerald, Kingsley and Umans, 2003) as shown in Figure 2.2. The damping response varies depending on the resistance to reactance ratio. As with induction machines with high rotor resistance, higher winding resistance results in a

poorer torque/slip ratio. For a slight change in speed, lower resistance results in increased

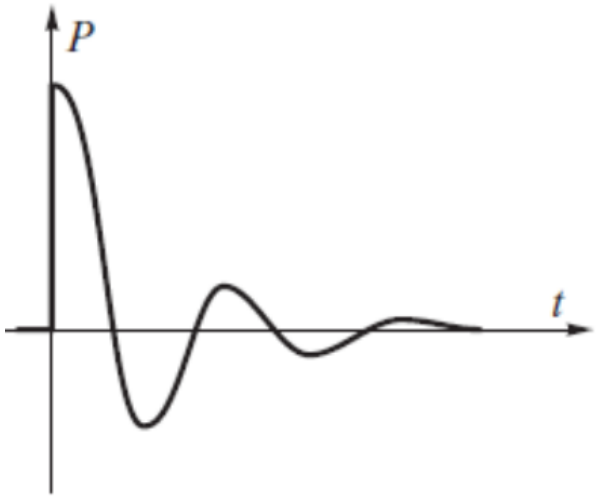

damping torque.

Figure 2.2 Power oscillations with damping (Fitzgerald, Kingsley and Umans, 2003)

It is possible for the rotor to accelerate or decelerate when it is perturbed from its equilibrium position. If dw>0, damping power is negative, effectively opposing acceleration; on the other hand, if dw<0, damping power is positive, supporting electrical power's opposition to slowing. In the absence of dampening, the rotor will ultimately pursue a different path and achieve synchronism without the unending oscillations known as hunting (Fitzgerald, Kingsley and Umans, 2003; Ceraolo and Poli, 2014).

2.3 Virtual Synchronous Machine (VSM)

Fundamentally, a VSM is a power electronics device that stores short-term energy and has a dispatching mechanism that allows it to operate like a synchronous generator (Cheema, 2020). VSM simulates the inertial and damping qualities of a synchronous machine, and it may either inject or absorb power into or from the grid in a manner similar to the injection or absorption of kinetic energy in synchronous generators (Pimprikar, Pawaskar and Kumar, 2018; Cheema, 2020). Because of these characteristics, a VSM is capable of reducing the frequency fluctuations that occur during transient periods. The VSM is comprised of an inverter, a frequency sensor, and a controller, all of

which work together to provide the switching signals required. Depending on the VSM application, a voltage source inverter or a current source inverter may be employed (Bollen *et al.*, 2009).

The VSM concept was originally centered on duplicating the dynamic features of a true synchronous generator (SG) for power electronics-based distributed generation and renewable energy systems (DG/RES), in order to benefit from the benefits of an SG in terms of stability improvement. The VSM concept may be used to a single DG or to a collection of DGs, depending on the situation. In contrast to the first use, which may be more ideal for individual owners of DGs, the second application is more cost-effective and simpler to regulate from the perspective of the network operator (Zhu, Wang and Zhu, 2021). The dynamic qualities of an SG allow for the adjustment of active power, the dependence of the grid frequency on the rotor speed, the highlighting of the spinning mass and dampening windings influence, as well as stable operation with a high degree of parallelism (Pimprikar, Pawaskar and Kumar, 2018; Cheema, 2020). The nominal state of charge (SOC) of the energy storage in a VSM should be operated at around 50 percent of its nominal capacity in a stationary condition, in order for the VSM to be capable of injecting or absorption power. The VSM operating states may be established depending on the SOC condition and the lower and higher limitations that have been set (for example, 20 percent and 80 percent of maximum charge). During periods when the SOC is within approximately these limits, the VSM operates in its active (VSM) mode; during periods when the energy in the system exceeds these limits, the VSM operates in its virtual load mode. The restrictions may be calculated depending on the energy storage technology that is being employed (Yuan *et al.*, 2016).

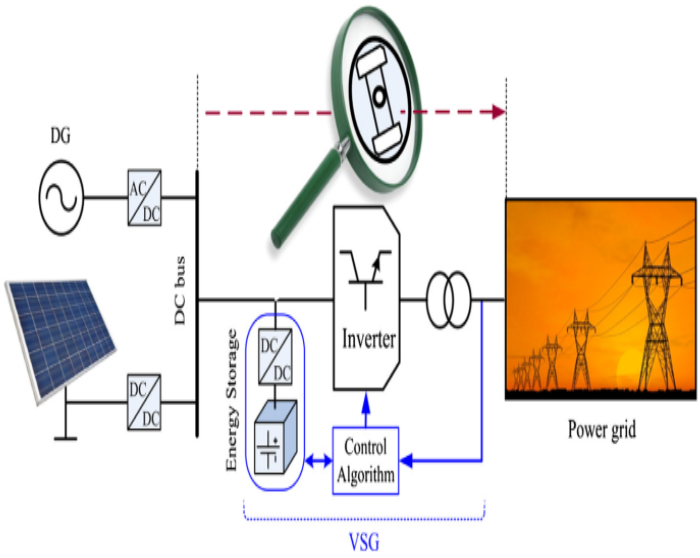

Figure 2.3 General Structure of VSM (Bevrani, Ise and Miura, 2014)

2.3.1 Operating Principle of VSM

The functioning of a VSM is functionally similar to that of an ideal synchronous machine, in that it may create or absorb active power by adjusting the output of the inverter, depending on the situation (Liang and Karim, 2016). When the load on the system is raised, the frequency of the system decreases, and the synchronous machine is activated, supplying the system with active power. If, on the other hand, the load is reduced, the frequency of the system will rise, and the synchronous machine will absorb active power from the system (Cheema, 2020), the system will become more efficient. The converter of the VSM system converts the dc voltage source into a series of regulated three-phase output voltages (V_0) with a frequency equal to the frequency of the alternating current system voltage. The active power transferred between the inverter and the alternating current system is produced in a manner similar to that of the synchronous condenser (Elsavad, Sarhan and Abdin, 2017) by adjusting the phase angle of the inverter output voltage (V_0).

i) If $F_{ref} > F_{grid}$, then active power is provided by the inverter.

ii) ii) If $F_{ref} < F_{grid}$, then the inverter consumes the active power

iii) If $F_{ref} = F_{grid}$, then there is no exchange of active power

Where, F_{ref} is reference frequency and F_{grid} is frequency of the grid measured.

The required power to be exchanged in between the grid and the VSM (P_{VSM}) is given by (Bevrani, Ise and Miura, 2014),

$$P_{VSM} = K_I \frac{d\Delta f}{dt} + K_D \Delta f \qquad \text{Equation 2.2}$$

Where, K_I =emulated inertia constant

K_D =damping constant

They are calculated as,

$$K_I = \frac{P_{rating}}{(\frac{d\Delta f}{dt})_{max}} \qquad \text{Equation 2.3}$$

$$K_D = \frac{P_{rating}}{(\Delta f)_{max}} \qquad \text{Equation 2.4}$$

Where P_{rating} is the nominal power rating of the VSM, $(\Delta f)_{max}$ is the maximum change in frequency and $\left(\frac{d\Delta f}{dt}\right)_{max}$ is the maximum ROCOF permitted in the system. The rating of VSM should be selected in such a way that, even in the worst probable transient condition, it can provide deficient power or consume excess power, as set up by boundary condition for frequency change and ROCOF (Liang and Karim, 2016; Mir and Senroy, 2020). The nominal rated power of the VSM, 'P_{rating}' should be 10% of the PV – hydro system's overall capacity. According to ISO standards 8528-5 for generating sets, the greatest deviation of frequency allowed during normal operating condition was ±2.5% i.e. 1.25 Hz (for 50 Hz system) and maximum ROCOF allowed was ±1% i.e. 0.5 Hz/s (for 50 Hz system). Also, during the transient operating condition, the maximum frequency

deviation allowed is ±15% i.e. for 50 Hz system, 7.5 Hz (Bevrani, Ise and Miura, 2014; Tamrakar *et al.*, 2015; Elsavad, Sarhan and Abdin, 2017).

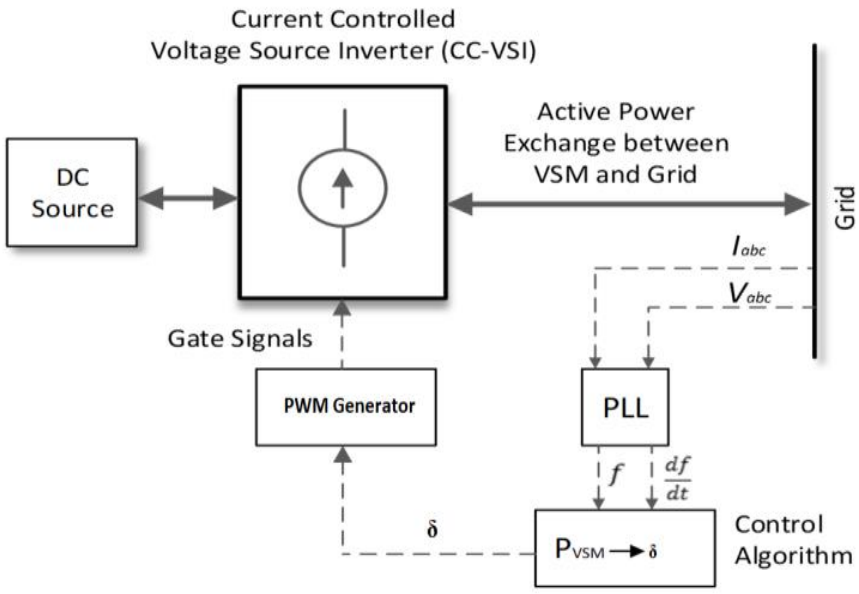

Figure 2.4 Operating principle of VSM (Tamrakar *et al.*, 2015)

2.4 Emulation of Synchronous Generator

The equation of motion of a synchronous machine is given as (Fitzgerald, Kingsley and Umans, 2003):

$$Tm - Te = \frac{2Hd^2\delta}{w_o dt^2} + \frac{K_d}{w_o}\frac{d\delta}{dt} \qquad \text{Equation 2.5}$$

Where; H= per unit inertia constant

Tm=mechanical torque in N.m

Te = electromagnetic torque in Nm

W_0= angular velocity of the rotor, mech. rad/s

K_d= Damping coefficient in pu torque/pu speed deviation

δ= angular position of the rotor in electrical rad/s

In equation 2.5 the part of the equation containing 'H' represents the inertial property of the synchronous machine and the part containing K_d represents the damping property of the machine.

From equation 2.2, compared with equation 2.5, an analogy can be derived between VSM and the synchronous machine. The part containing 'K_I' in equation 2.2 is analogous to the part containing 'H' in equation 2.5 i.e. inertial property of the machine. The part containing 'K_d' in equation 2.2 is analogous to the part containing 'K_d' in equation 2.5 i.e. damping property of the machine.

In order to emulate the inertial and damping properties of a synchronous machine, VSM requires the proper selection of the constants K_I and K_d which are calculated using equation 2.3 and 2.4 (Bevrani, Ise and Miura, 2014). Inertia and damping emulation control need to be closely analyzed which are described below briefly.

2.4.1 Inertia emulation control

The inertia is related to the power with the derivative of the frequency change. Accordingly, the part "K_I ($d\Delta f/dt$)" in equation 2.2 is responsible for the emulation of inertia in the system. It directs the inverter to exchange the power according to the rate of change in frequency just like the rotating parts do in the real synchronous machine. By exchanging the power, the rate of change in frequency of the system can be impeded; and hence inertia can be said to be emulated (Zhang *et al.*, 2019). The amount of inertia to be emulated can be varied by changing the value of 'K_I' (Fitzgerald, Kingsley and Umans, 2003; Cheema, 2020).

2.4.2 Damping emulation control

Similarly, the damping effect is related to the proportional deviation of frequency from the reference value. Hence, the part 'K_d (Δf)' will be emulating the damping effect into the system. This allows the inverter to inject or absorb power into the system according to the change in frequency, in a similar way as the damper winding would have done(Wang *et al.*, 2018). By changing the value of 'K_d', the amount of damping to be emulated can be varied (Fitzgerald, Kingsley and Umans, 2003; Cheema, 2020).

2.5 Control Scheme of VSM

There are various kinds of control schemes of VSM and two of the schemes are described briefly below.

2.5.1 Conventional Method

2.5.1.1 VSM with Hysteresis Band Current Control (HBCC)

Hysteresis Band Current Control (HBCC) is a kind of instantaneous feedback control system in which the actual current signal is compared with the reference current signal of the inverter using a hysteresis current controller (Tamrakar *et al.*, 2016). Whenever the actual current signal is greater than the reference current signal within a particular range, we may alter the switching state of the inverter, which will change the direction of the actual current signal, allowing it to follow the reference current signal (Jun and Dazhi, 2009). A number of benefits of hysteresis current control include its rapid reaction time, internal current limiting capability, and stability. Based on the above benefits, hysteresis current control is extensively employed in power inverters, alternating current drives, active power filters, variable speed drives, and variable speed motors (Jun & Dazhi,2009; Tamrakar et al., 2016).

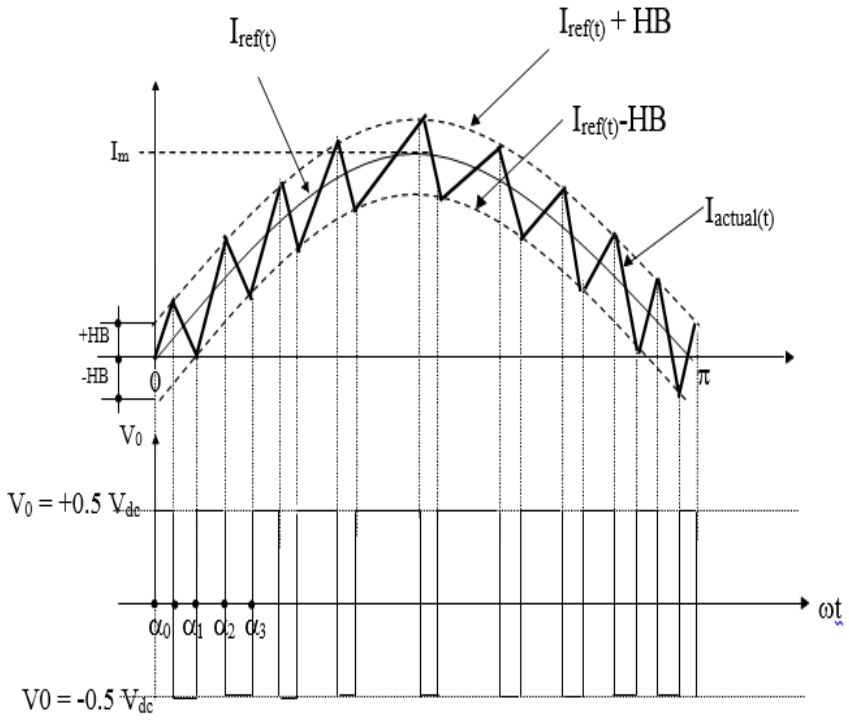

Figure 2.5 Switching instants and waveforms of HBCC inverter (Tamrakar *et al.*, 2016)

With a closed-loop control system, a hysteresis current controller is created and implemented. The switches in an inverter are controlled by an error signal, denoted by the symbol e(t). When the required current, $I_{ref(t)}$, is greater than the actual current, $I_{actual(t)}$, then an error has occurred. When the fault exceeds a certain threshold, the transistors are turned off, causing the current to decrease. When the error falls below a certain threshold, the current is compelled to rise. The Hysteresis Band refers to the range of the error signal that directly determines the amount of ripple in the output current from the inverter. The error signal range is measured in milliseconds. Having known as the Lower Hysteresis Limit and Upper Hysteresis Limit, these two hysteresis limits are directly related to an offset from the reference signal and are thus referred to as such. Even if the reference current is changing, the current is compelled to remain within these limitations.

The turn-on and turn-off conditions for the inverter switches are:

Upper switch off: $(I_{actual(t)} - I_{ref(t)}) > HB$.

Lower switch off: $(I_{actual(t)} - I_{ref(t)}) < -HB$.

Where, HB= Hysteresis Band

The inverter's switching frequency is determined by the breadth of the hysteresis band in which it operates. The switching frequency rises in proportion to the narrowing of the band width. According to the switching capabilities of the inverter (Jun and Dazhi, 2009; Tamrakar *et al.*, 2016), an appropriate bandwidth should be set. The fixed hysteresis band is a fairly straightforward and straightforward design to build. This high frequency puts a significant amount of stress on the switches and results in significant switching losses. Inductors have a maximum rate of change of current that is too low to keep up with the sharp current variations that occur at high frequencies when the inductance is too great. Because of the modest inductances that have been chosen, the rates of change of current will be very fast. High switching frequencies are produced as a consequence, resulting in significant losses in the semiconductor switches (Jun and Dazhi, 2009). There is also a rise in the levels of electromagnetic interference as a result of this, and it is necessary to do extremely fast comparisons between real current and the hysteresis limits.

The block diagram of VSM with hysteresis band current control technique is shown in Figure 2.6 (Tamrakar *et al.*, 2016). The grid frequency drops as the active power of the load rises. The frequency is measured and compared to a standard value. The magnitude of the reference current i_{abc} is calculated using the error signal received so far $i_{abc(ref)}$. The hysteresis band current controller compares the actual currents through the VSM branch with the reference currents and produces gate signals to turn on and off the switch numerous times in a cycle, ensuring that the actual inverter current i0(actual) matches the reference current iabc(ref) within a narrow hysteresis region.

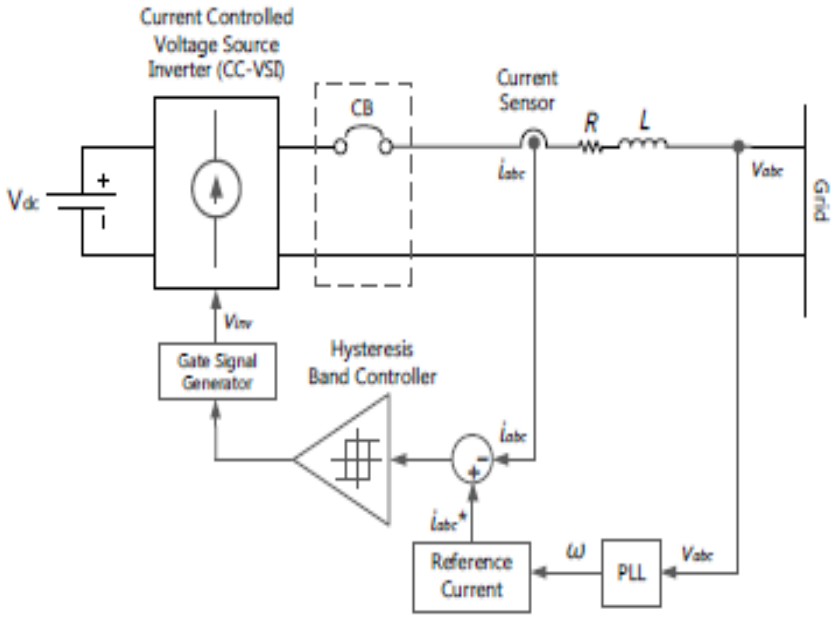

Figure 2.6 VSM with HBCC inverter (Tamrakar *et al.*, 2016)

2.5.2 Proposed Method of Control

2.5.2.1 VSM with Power Angle Control

The basic idea of power angle control is to vary the phase displacement angle between the three-phase voltage of the inverter and the three-phase voltage of the grid. The voltage difference between the three-phase voltage of the inverter and the three-phase voltage of the grid will be placed over an inductance in each phase. The larger the phase displacement angle the larger the voltage difference across the inductor which results in a higher current through the inductor.

The active power is given by (Ceraolo and Poli, 2014):

$P=(EV\sin\delta)/X$ Equation 2.6

Where, E=phase to phase rms voltage of inverter

V=rms phase to phase voltage of grid

δ =phase displacement angle

X=reactance in each phase

Although the fundamental idea for power angle control is to find the phase angle of the voltage of inverter terminal with respect to grid voltage and then injecting the calculated P_{vsm} to grid based upon this angle, the approach of generating this angle varies from one method to another. The novel approach that has been used here is shown in Figure 2.7.

The grid's frequency is determined using the Phase Locked Loop (PLL) method (Ceraolo and Poli, 2014). The error is then calculated by comparing this measured frequency with reference frequency where the reference frequency is taken as 50Hz. The P_{vsm} calculation block takes this error signal and outputs the required power (P_{vsm}) to be injected into grid as shown in Figure 2.7. It calculates P_{vsm} based on (2.2) which is dependent on the ROCOF and change in frequency. The required power to be injected (P_{vsm}) and the power actually injected by VSM at the instant are passed as inputs to angle controller block which is based on the linearized model of swing equation. The output angle from the angle controller block, along with modulation index and grid frequency is then passed to the three-phase sine generator which produces reference signals to generate the PWM signals. The modulation is fixed constant as this thesis is ideally dealing with active power control only rather than reactive power. After this, the PWM generator generates six gate pulse signals using sinusoidal reference signal and triangular carrier wave, which is then sent to inverter for its switching operation. Finally, the inverter injects/absorbs necessary calculated power (P_{vsm}) to/from grid based upon its switching pattern which is determined by gate pulse signals (Elsavad, Sarhan and Abdin, 2017).

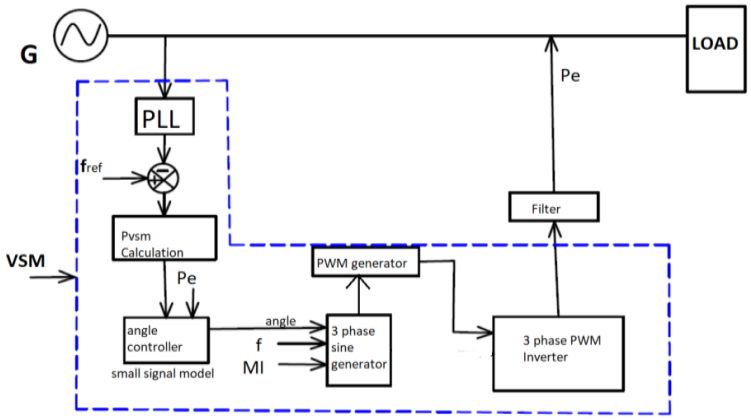

Figure 2.7 Angle control scheme based on small signal model

Angle controlling scheme is based on swing equation(Fitzgerald, Kingsley and Umans, 2003) as mentioned below:

$$\frac{H}{\Pi f_0}\frac{d^2\delta}{dt^2} = P_m - P_{max}sin\delta - D\frac{d\delta}{dt} \qquad \text{Equation 2.7}$$

Where H is inertia constant due to mass of rotating body, D is damping constant due to damper winding, δ is power angle in electrical radian, P_m is the mechanical power, which is actually the power (P_{vsm}) to be injected by VSM, $P_{max}sin\delta = P_e$ is the electrical output power.

Linearizing equation 2.7 at $\delta = \delta_0 + \Delta\delta$,

$$\frac{H}{\Pi f_0}\frac{d^2\Delta\delta}{dt^2} + D\frac{d\Delta\delta}{dt} + P_{max}cos\delta_0\Delta\delta = P_m - P_e \qquad \text{Equation 2.8}$$

The block shown in Figure 2.8 is constructed using Equation 2.8 which gives the $\Delta\delta$ as output.

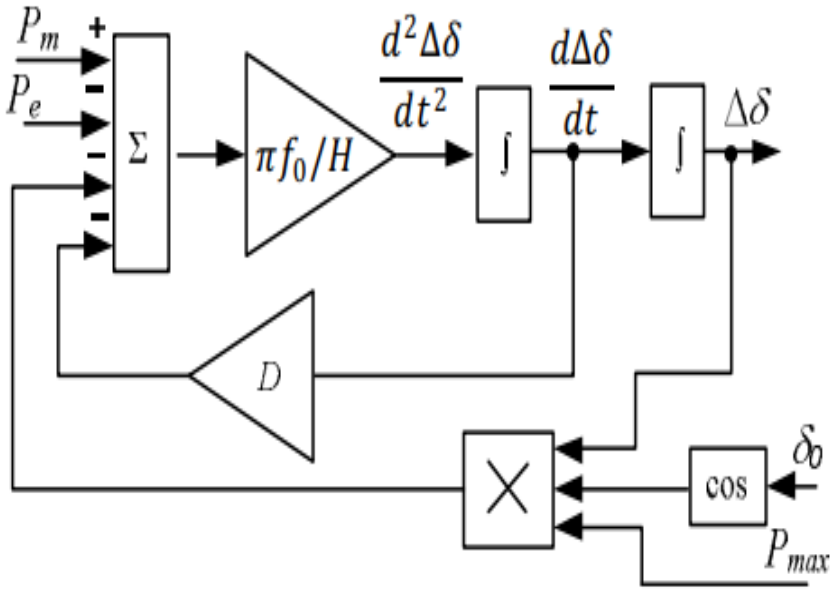

Figure 2.8 Power angle controller (Elsavad, Sarhan and Abdin, 2017)

2.6 Maximum Power Point Tracking (MPPT)

When it comes to photovoltaic (PV) solar systems, maximum power point tracking (MPPT), also known as power point tracking, or simply power point tracking (PPT), is a method that is often employed to optimize power extraction under all situations (Haji and Genc, 2018).

It is possible to study the I-V curve to determine the output efficiency of solar cells because of the intricate connection between temperature and total resistance that exists in solar cells. The MPPT system's primary function is to sample the output of the PV cells and apply the appropriate resistance (load) in order to produce the most power possible under any given environmental circumstances (Haji and Genc, 2018). When used in conjunction with an electric power converter system, MPPT devices generally offer voltage or current conversion, filtering, and control for driving a variety of loads including power grids and batteries (Sahay and Yadav, 2018).

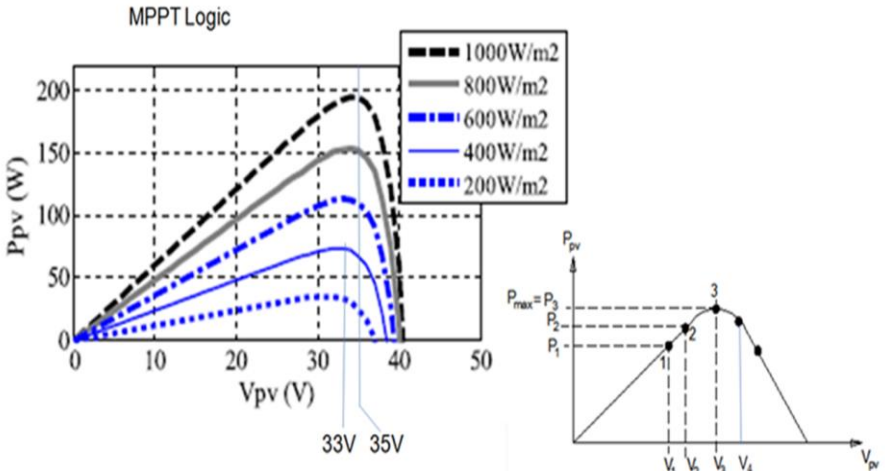

Figure 2.9 PV curves at different irradiances

For Maximum Power Tracking, Perturb and Observe (P and O) algorithm is used. In this technique, when a minor perturbation is introduced in voltage, it causes the power variation of the PV module as shown in P-V curves (Kollimalla and Mishra, 2014). The PV output power is periodically measured and compared with the previous power. If the output power increases, the same process is continued. Otherwise, perturbation is stopped at the previous point (Haji and Genc, 2018). For example: starting from V_1, Power increases up to perturbed value V_3 and power decreases at the next perturbed value of V_4.

2.7 DC-DC Boost converter

The simulation circuit of the boost converter is shown in Figure 2.10. It consists of an IGBT switch, an inductor, and a diode. When the switch is in ON state the inductor stores charge because the diode is reverse biased. When the switch is in OFF state the inductor releases energy and provides current to the load (Sinha *et al.*, 2018).

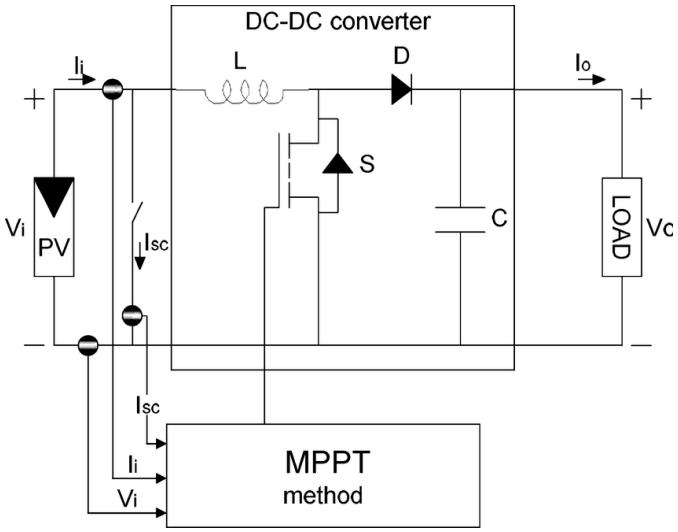

Figure 2.10 DC-DC boost converter

When the switch is ON, the inductor stores energy and the load gets power from the previously charged capacitor.

When the switch is OFF, the inductor releases energy (stored in the previous cycle) and supplies power to the load and charging current to the capacitor.

Current at the end of the switch on (Sahu, Verma and Nema, 2016),

$$I_{\mathrm{L}}(+) = \frac{1}{L} \times V_{in} \times k \times T_s$$

Where $k = \frac{Ton}{Ton + Toff}$

T_s = cycle time

I_L=Current through inductor

Current at the instant of switch off (Sahu, Verma and Nema, 2016),

$$I_L(+) = \frac{1}{L} \times (V_{in} - V_{out}) \times (1 - k) \times T_s$$

Current at the end of switching on should be equal to the current at the instant of switching off

i.e. $\frac{1}{L} \times Vin \times k \times Ts = \frac{1}{L} \times (V_{in} - V_{out}) \times (1 - k) \times T_s$

$\frac{V_{out}}{V_{in}} = \frac{1}{1-k}$, k<1

So, $V_{out} > V_{in}$

Hence, the name converter is named as boost converter.

2.8 dq0 to abc Transformation

The Inverse Park Transform is implemented via the dq0 to abc transformation. A rotating reference frame is converted to an abc reference frame by using the Inverse Park Transform block, which changes the time-domain direct, quadrature, and zero components to the components of a three-phase system in the rotating reference frame. In a balanced system, the zero component has the value of zero, as well. The dq0 to abc transformation of the MATLAB Simulink block is supported by two different Parks transformation protocols. At t=0, one is rotating a frame that is aligned with the reference axis. It is sometimes referred to as the cosinus-based Parks transformation or the Parks transformation using cosinus. Another option is to use a rotating frame that is 90 degrees behind the references. Sinus-based Parks transformation is the name given to this particular sort of Park's makeover. In PV model, we have implemented the Parks transformation based on sinuses. The equation 2.8 (Fitzgerald, Kingsley and Umans, 2003) gives the formula for the inverse sinus-based Parks transformation, which is also known as the Parks transformation. Figure 2.11 shows a phasor diagram relating abc and dq frame where a, b and phasors are phased at 120^0 and d and q phasors are placed at 90^0 phase difference to each other.

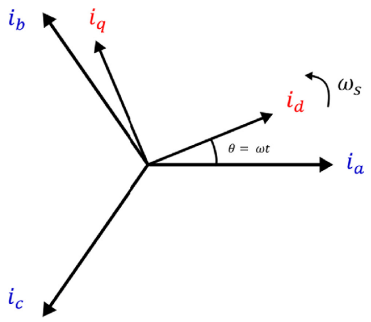

Figure 2.11 dq and abc frame

$$\begin{bmatrix} a \\ b \\ c \end{bmatrix} = \begin{bmatrix} \cos(\theta) & \sin(\theta) & 1 \\ \cos\left(\theta - \frac{2\pi}{3}\right) & \sin\left(\theta - \frac{2\pi}{3}\right) & 1 \\ \cos\left(\theta + \frac{2\pi}{3}\right) & \sin\left(\theta + \frac{2\pi}{3}\right) & 1 \end{bmatrix} \cdot \begin{bmatrix} d \\ q \\ 0 \end{bmatrix}$$

Equation 2.8

Where, θ is the position of rotating reference frame.

The input signals to the dq0 to abc transformation blocks are I_d, I_q, I_0 and position of the rotating reference frame($\theta=\omega t$). I_d and I_q are found from I_d and I_q calculation blocks respectively. Io is set to zero since the zero sequence component for a balanced three phase system is zero. The position of the rotating reference frame is found from Phase Locked Loop (PLL). The output of dqo to abc transformation is the reference three phase abc current i.e. $I_{abc(ref)}$.

CHAPTER THREE: RESEARCH METHODOLOGY

3.1 Methodology Approach

For the successful completion of the research, various works have been performed which are presented in order of occurrence as shown in Figure 3.1. First of all, a hydro system of 150 kVA has been modelled and simulated. Then, a PV array of capacity around 10 % of hydro system has been added to the former system. The main goal is to create a system that lacks enough inertia, rather than creating economically optimized system, during transient condition to bring transient stability to the system. i.e the system containing hydro and PV is designed in such a way that when there is 0.2 pu load switching takes place, the frequency will go down by more than 15%, thereby making transient instability. Accordingly, the synchronous generators has been modelled and a 10 kW PV would be added. Then, the load was switched on to create the transient situation without using VSM. Then, a VSM was designed and connected to the system to check the frequency deviation within nominal range. The VSM has been controlled by power angle control strategy.

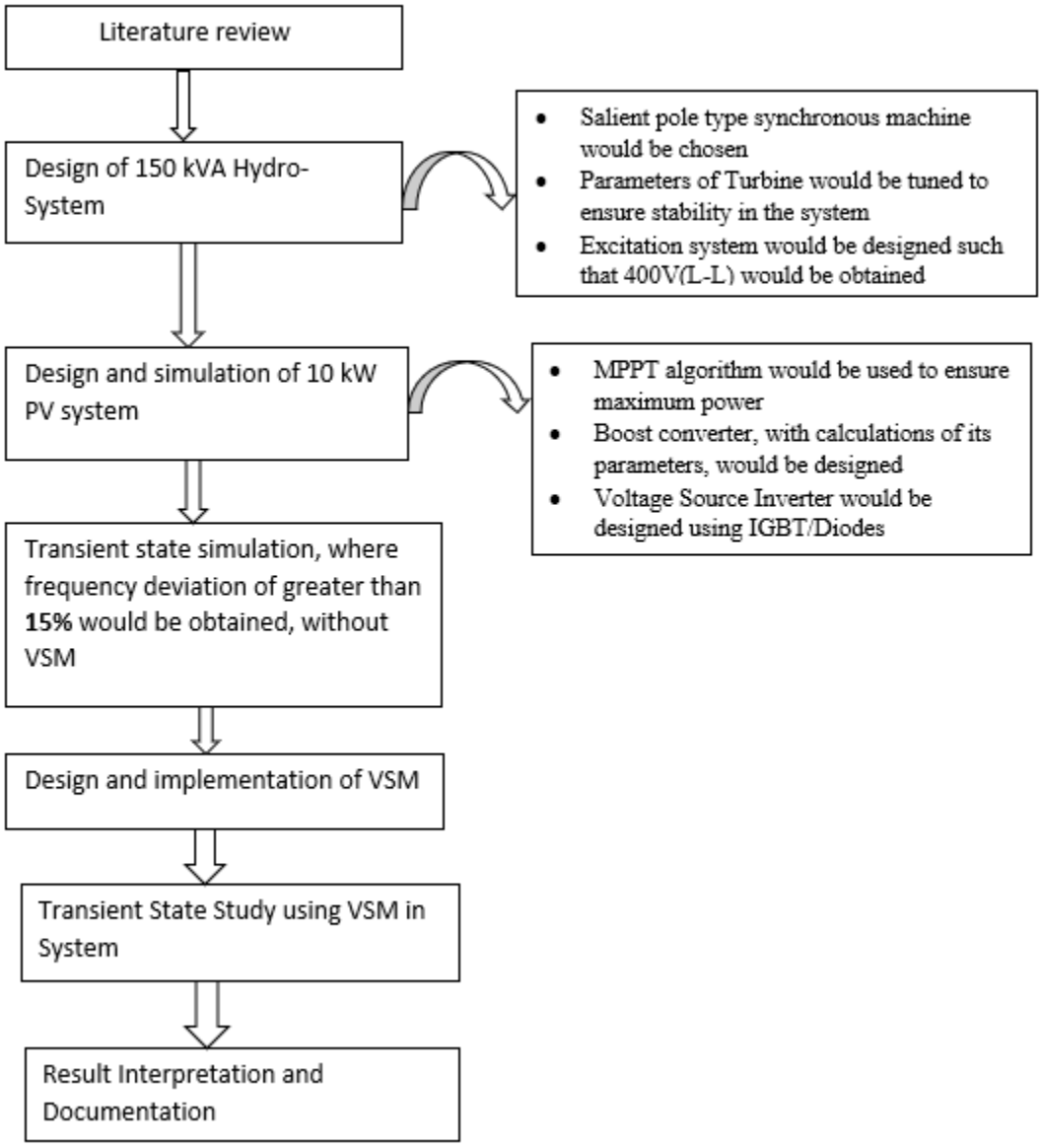

Figure 3.1 Methodology Approach

3.2 Design and Modelling of Hydro-System

A MATLAB block named synchronous machine pu standard has been taken and the capacity is made to be equal to 150 kVA. A lot of time has been dedicated to control the turbine and governor, especially in its P and I parameter of PI controller. Finally, suitable value of P and I with appropriate gate constant was selected and the generator system was designed. Also, the output from generator was distorted voltage form and excitation system was properly tuned to make the smoother output.

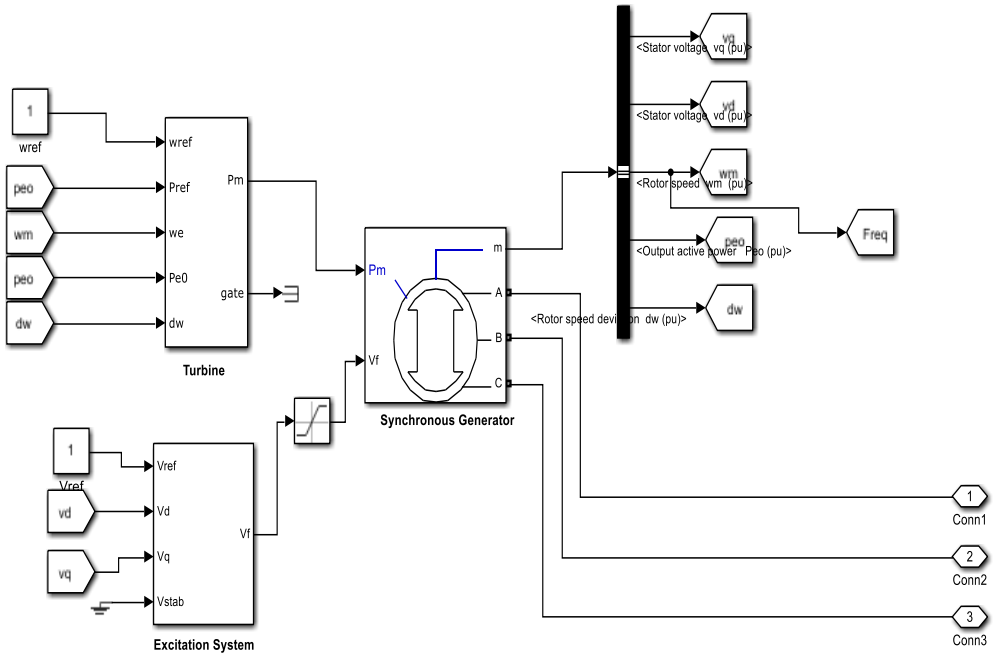

Figure 3.2 Design and model of Hydro-system

3.3 Design of 10 kW PV System

For the design of PV System, first of all appropriate number of models have been selected. To produce a line to line voltage of 400V, from the literature review(Electronics, Circuit and Simulation, 2016; Ceraolo and Poli, 2014), it is required to have a dc voltage of 600V. For the same purpose, a PV array with 3 parallel strings each with 11 models in series has been chosen. The irradiance variation has been taken into account. The PV array is followed by boost converter, giving 600V output, whose gate signals are driven by MPPT technique using P and O algorithm. Then, this dc power is transformed to three phase ac using three phase full bridge converter. This converter is controlled by hysteresis band controller. A significance amount of time is required to model this system as it requires suitable selection of passive parameters like inductance and capacitance.

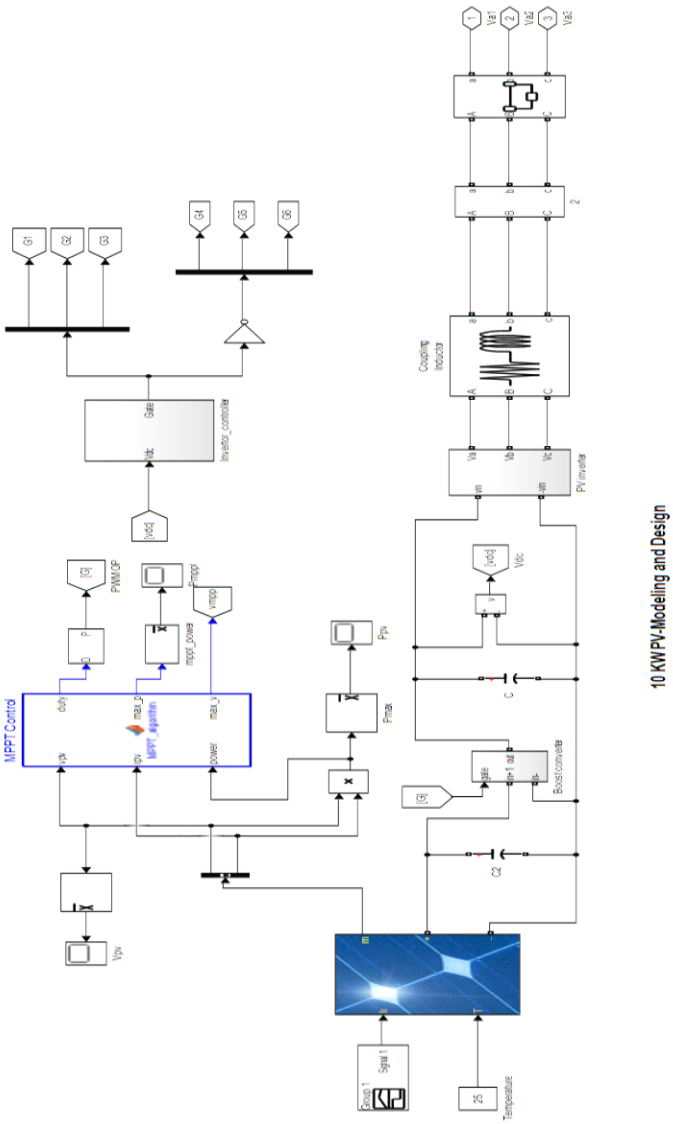

Figure 3.3 Design and model of 10 kW PV-System

3.3.1 Boost Converter Design:

The boost converter designed in Simulink is shown in Figure 3.4. The switching frequency of 20 kHz is chosen as IGBT/Diodes is used in this circuit(Ceraolo and Poli, 2014; Li, Chen and Jiang, 2020). It will work efficiently at this frequency. Average voltage during irradiance is assumed to be 545 V and the output voltage from boost converter is 600V. An efficiency of 94% is chosen as the practical efficiency lies in this range.

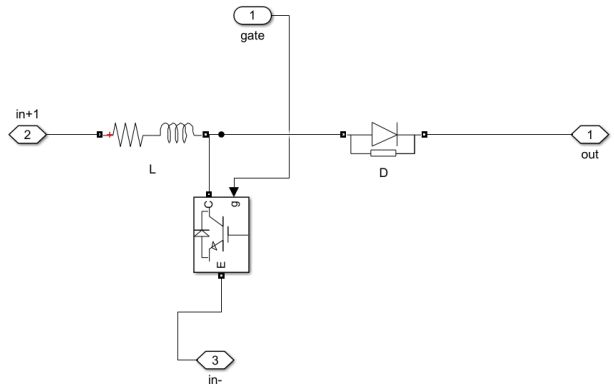

Figure 3.4 Boost converter in Simulink

Switching Frequency (f_s) = 20 kHz

Boost converter source voltage (V_s) = 545 V

Boost converter output voltage (V_d) = 600V

Power Output (P) = 10 kW

Then,

Calculation of Duty Cycle

Duty Cycle (D) =$1 - \left(\frac{Vs}{Vd} \times n\right)$

$=1-\left(\frac{545}{600}\times 0.94\right)$

$=0.15$

Calculation of Inductance:

$L \geq \frac{V_{s(min)}\times D}{f_s * \Delta I_L}$ where I_L is inductor current.

Let us find ΔI_L,

$V_{s(min)}$ =545 V

ΔI_L=(20% to 40%) of I_L

Taking ΔI_L = 30% of I_L

Where $I_L = \frac{P}{V_d} = \frac{10000}{600}$ = 16.67 A

So, ΔI_L = 30% of 16.67 A

= 5 A

Now, $L \geq \frac{545\times 0.15}{20\times 1000\times 5}$

$L \geq 7.98*10^{-4}$

$L \geq 0.8$ mH

We have chosen 1 mH inductor in our boost converter.

Calculation of Capacitance:

$$C \geq \frac{I_{o(max)} \times D}{f_s * \ \Delta V_d}$$

$I_{0\,(max)} = I_L = 16.67$ A

ΔV_d =(1% to 5%)of V_d

Taking 1% we get,

ΔV_d = 1% of 600 V

= 6 V

Again,

$C \geq \frac{16.67 \times 0.15}{20 \times 1000 \times 6} \geq 2.10 \times 10^{-5}$

We have chosen 4.4×10^{-4} C Capacitor in our boost converter.

3.3.2 PV Inverter Controller Design

Hysteresis Band Controller has been used to generate gate signals for the inverter bridges. The voltage of boost capacitor (V_{dc}) is compared with the maximum point voltage (V_{mpp}) and the error signal is passed to PI Controller, where it generates a signal proportional to the d component of current (i_d). Since, the PV inverter produces active power only, this d component of current ($i_{d)}$ would be proportional to the active power of the PV system. Then, id0 frame is converted to abc frame to produce reference sinusoidal signal. This reference sinusoidal current is then compared to the actual current produced by inverter and the error is passed to hysteresis band relay where the band is ±5 % of the peak value of current. Then, the output pulse of hysteresis band is the PWM to be fed to the inverter.

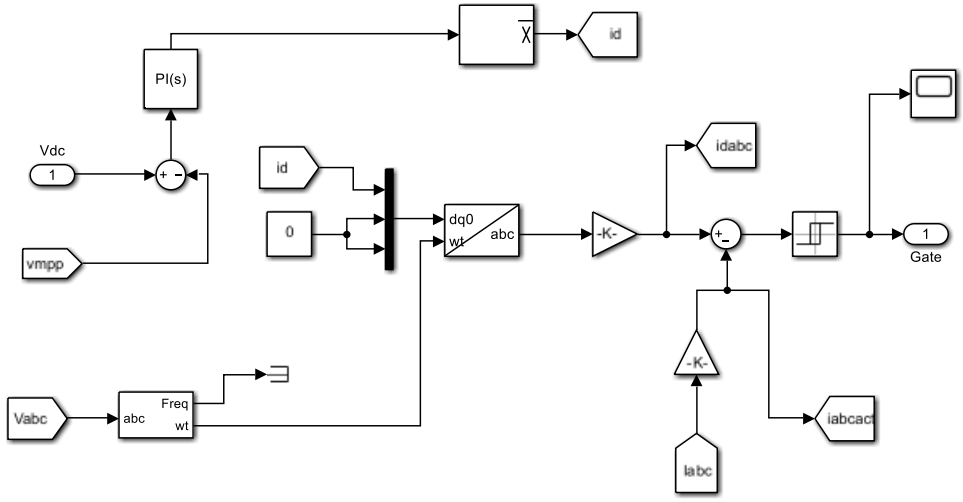

Figure 3.5 PV inverter controller

3.3.3 PV Inverter

Three phase PV inverter has been designed using 6 IGBT/ Diodes. The gates signals will be generated from hysteresis band controller. The Inverter works on 120 degree conduction mode. Then, this ac output is passed to grid through filter circuit.

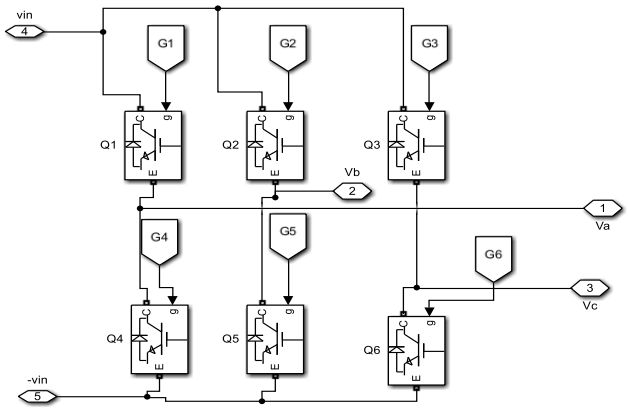

Figure 3.6 PV inverter

3.4 Load System

The load in this thesis consists of only active load as this project deals with the frequency stability rather than voltage stability. Since, the frequency is mostly affected by active power only, active load is considered. The 0.4 pu load is in operation all the time whereas 0.2 pu load is switched on after 3 seconds of operation automatically with three phase breaker and the transient condition is then started.

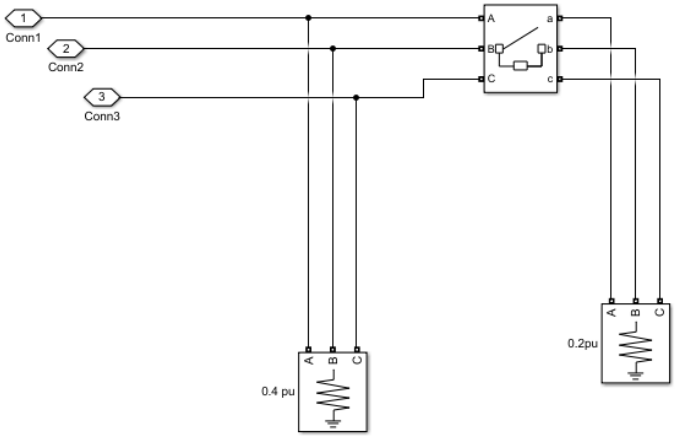

Figure 3.7 Three phase active load

3.5 VSM Modelling and Design

The frequency of the grid is sensed using Phase Locked Loop (PLL) block of Simulink and this frequency is passed to power calculation block where it calculates the power based on Equation 2.2. Then, the calculated power is passed to angle controller block, which is based on Equation 2.8**.** This calculated angle, along with modulation index and frequency of grid, is passed to three phase sine generator, which produces three phase references sinusoidal signal for sinusoidal PWM. After this, the two level PWM block produces six PWM pulses and is passed to inverter through activation circuit. The activation circuit activates VSM only when there is change in frequency by more than

2.5%. The power corresponding to the angle is then exchanged between VSM and the grid.

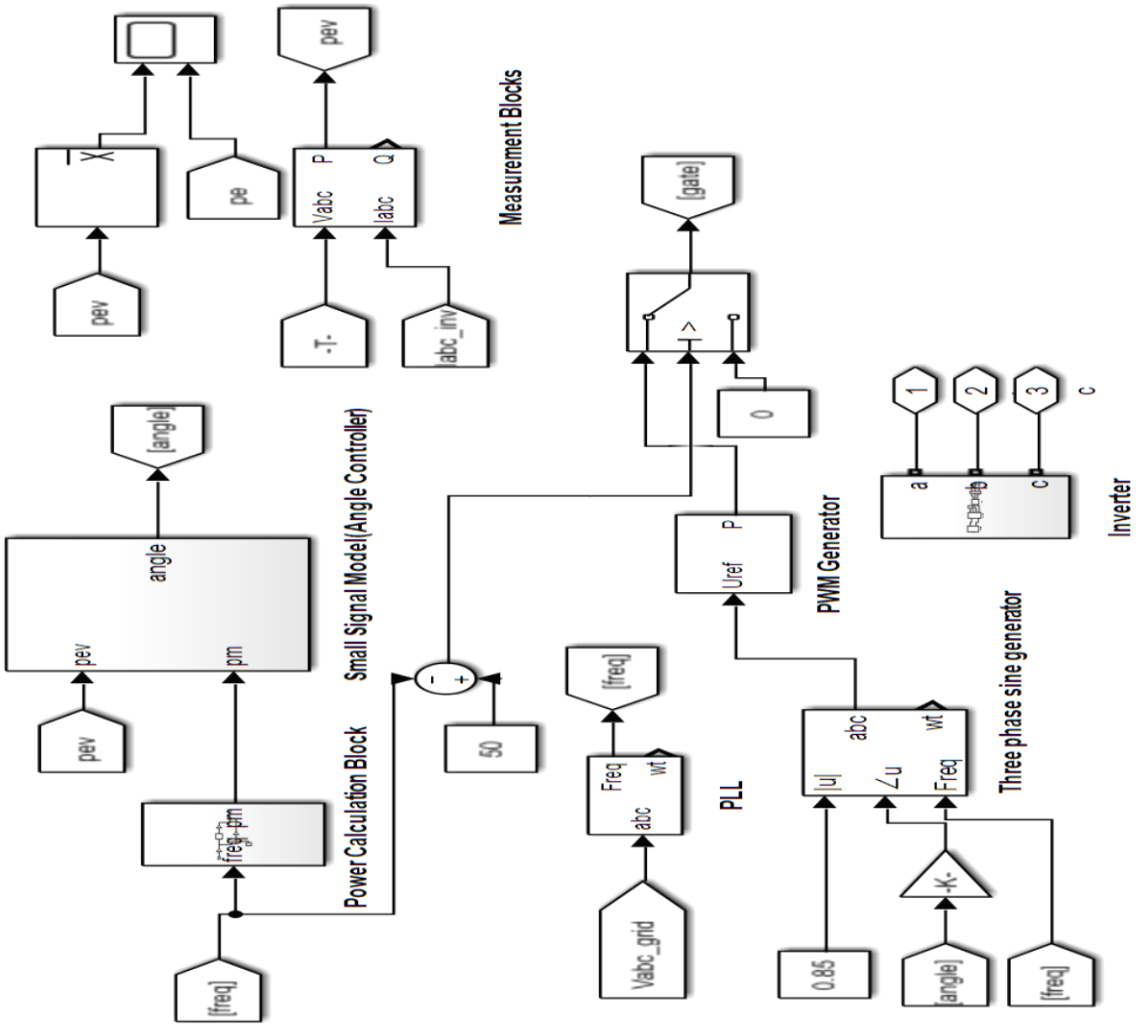

Figure 3.8 Overall parts of VSM in Simulink

3.5.1 Design of Power Calculation Block

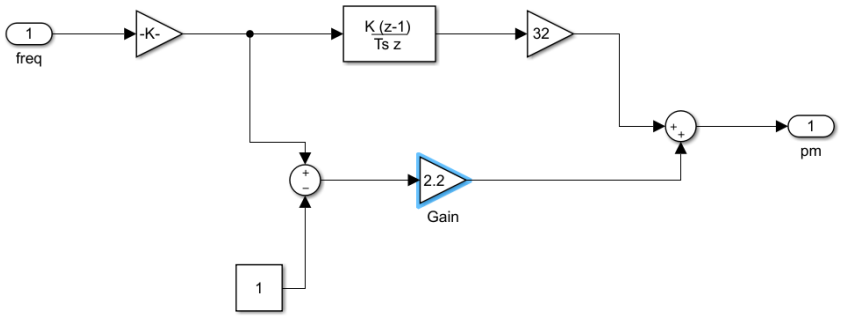

Figure 3.9 Power calculation block

This block is based on following equation.

The required power to be exchanged in between the grid and the VSM is given by,

$$P_{VSM} = K_I \frac{d\Delta f}{dt} + K_D \Delta f$$

Where, Where K_I =emulated inertia constant

K_D =damping constant

They are calculated as,

From literature study as mentioned in earlier section,

Rating of VSM P_{rating}= 10% of System rating=0.1*160=16kW

Maximum change in frequency= 7.5 Hz (15% of 50Hz)

Maximum ROCOF =0.5Hz/s (1% of 50Hz/s)

$$K_I = \frac{P_{rating}}{(\frac{d\Delta f}{dt})_{max}} = \frac{16}{0.5} = 32$$

$$K_D = \frac{P_{rating}}{(\Delta f)_{max}} = \frac{16}{7.5} = 2.3$$

3.5.2 Angle Controller Block

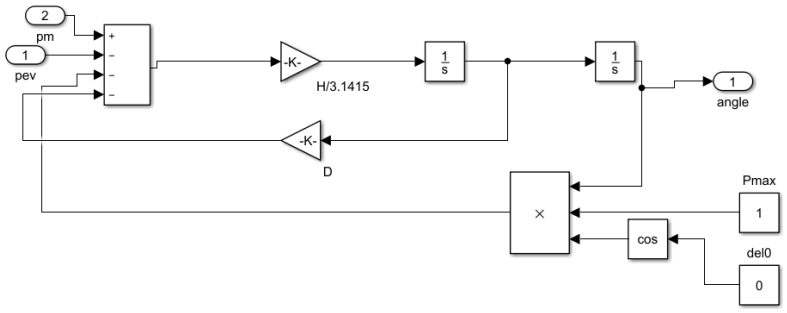

Figure 3.10 Angle controller in Simulink

This block generates the angle requires by VSM inverter. Actually, this angle is proportional to the active power to be exchanged by VSM with the grid. As mentioned in earlier section, this block is based on following equation:

$$\frac{H}{\Pi f_0}\frac{d^2\Delta\delta}{dt^2} + D\frac{d\Delta\delta}{dt} + P_{max}cos\delta_0\Delta\delta = P_m - P_e$$

Where, H= 2 to 4 for typical hydro generator and we have chosen 3.

Value of damping constant D is 2.3 as calculated before.

3.5.3 VSM Inverter

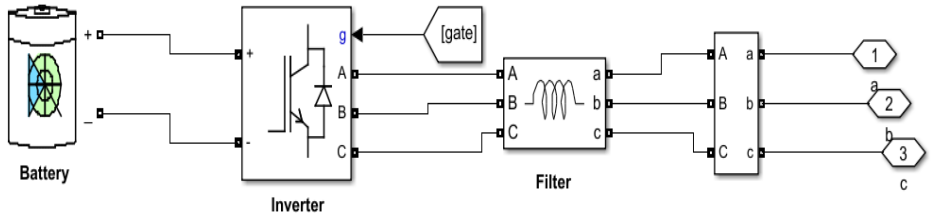

Figure 3.11 VSM inverter

The universal bridge from Simulink is taken and converted to three phase voltage source inverter with IGBT/diodes. The gate signals are produced by PWM generator. The battery of 600V is chosen so that the modulation index of 0.85 will produce a three phase line to line voltage of 400V in ac side. Then, the ac current is then passed to the grid through filters. The Lead acid battery is chosen because of the requirement of deep current discharge since the VSM will operate only for a few seconds. The Ah of the battery will be low due to this (Damon, 2003; IEEE-SA-Standards-Board, 2014).

Calculation of battery rating:

VSM Capacity=16 kW

DC voltage=600V

Maximum Current=16000/600=26.67A

Assuming VSM operates for a maximum of 30 seconds in one transient state,

Ampere hour rating of battery=26.67*30/3600=0.22Ah

But the State of Charge (SOC) of battery during normal state=50%,

Ampere hour rating =0.22/0.5=0.44 Ah

Assuming factor of safety=2,

Ampere hour rating of battery=0.88Ah =1Ah (near standard rating)

CHAPTER FOUR: RESULTS AND DISCUSSION

Simulation is subdivided into two cases. In first case (Case-I), the system is simulated without connecting VSM and the transient results are analysed. In second case (Case-II), the system is simulated with the involvement of VSM in the system.

4.1 Case-I

From Figure 4.1, the system consists of only hydro and PV. The 0.4 pu load is switched on continuously whereas 0.2 pu is load is switched on at t=3s and the transient state starts from here. The waveforms of frequency, voltage and current are shown and described in following section.

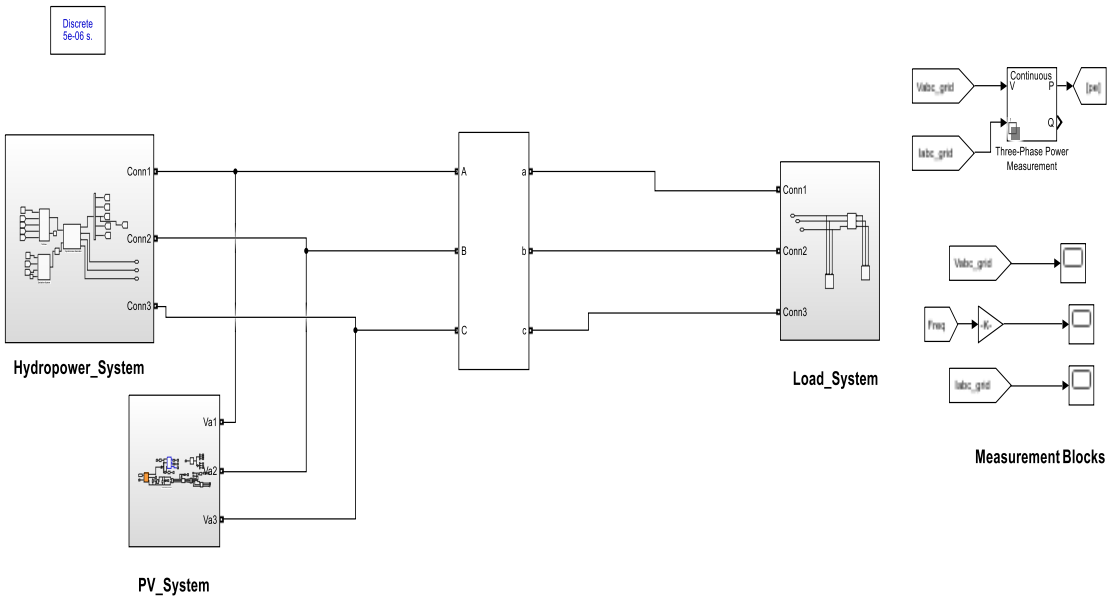

Figure 4.1 System during Case-I

From Figure 4.2, when a 0.2 pu load is switched on at time t=3sec, the frequency drops to 0.81 pu (40.5 Hz), which is about 19% deviation from nominal frequency. This is due to the mismatch between input and output power. The kinetic energy stored in the rotating part present in the grid is not enough to provide transient stability to the grid. Since the recommended tolerability is 15%, the transient stability is not maintained when this system alone is used without using VSM.

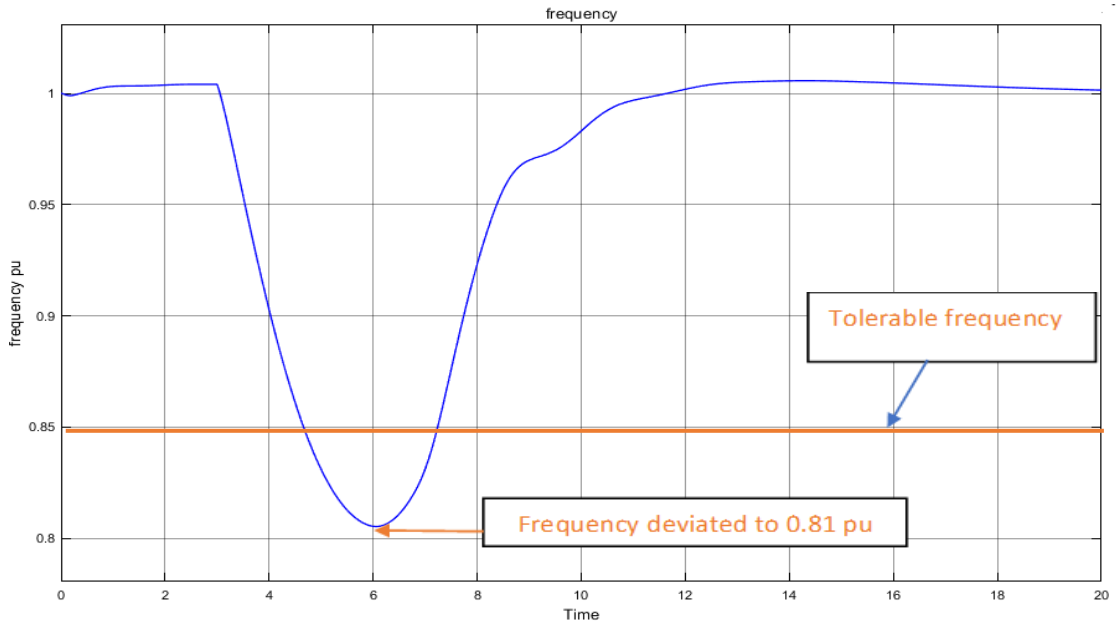

Figure 4.2 Frequency of the system during transient condition

Figure 4.3 shows the magnified form of the grid current waveform from (2.99 to 3.05) seconds which shows that the current is sinusoidal and increased from 0.4 pu to 0.6 pu at t=3 seconds. From it, it can be understood that current is increased after the load is switched on at t=3 seconds. At the instant of switching on, current is slightly disturbed but it is recovered to normal form after some seconds.

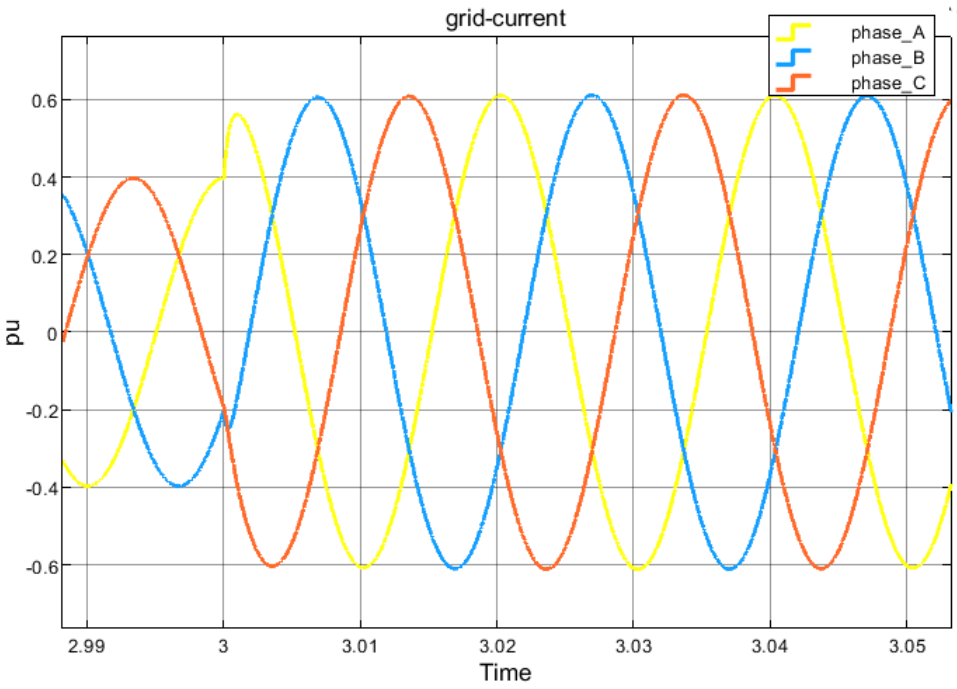

Figure 4.3 Current of the grid (VSM is not used)

Figure 4.4 shows the magnified form of the grid voltage from (15.57 to 15.62) seconds which shows that the voltage is of normal value and sinusoidal. When there is instant increase in load, the current will be increased on the same proportion instantly and the voltage drop increases. It will take some time to the excitation system to bring the voltage back to normal value.

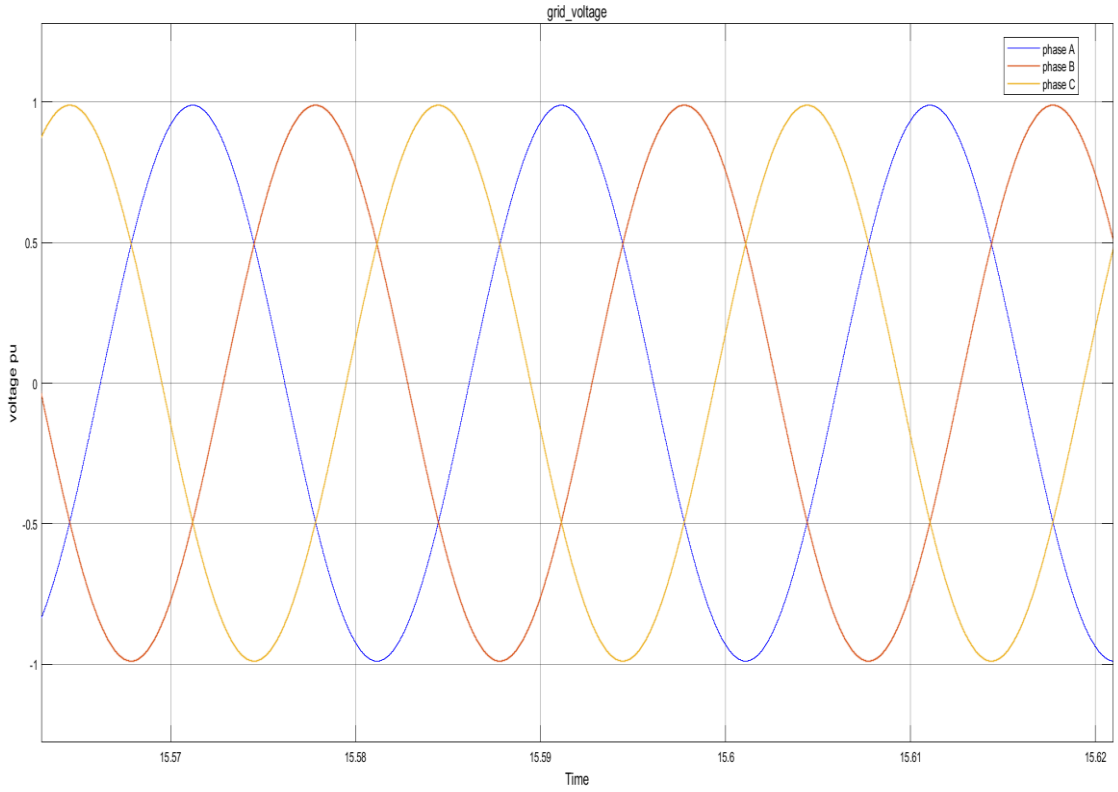

Figure 4.4 Voltage of the grid (VSM is not used)

4.2 Case II

The system is shown in Figure 4.5. The same previous load is switched on in the same manner but the VSM is also connected to the system. Since the VSM is connected and comes into operation when frequency changes by more than 2.5%, the VSM will give power to the load at the transient condition for a very small period of time and the transient stability of the system will then be improved. The waveforms of frequency, voltage and current are shown and described in following section.

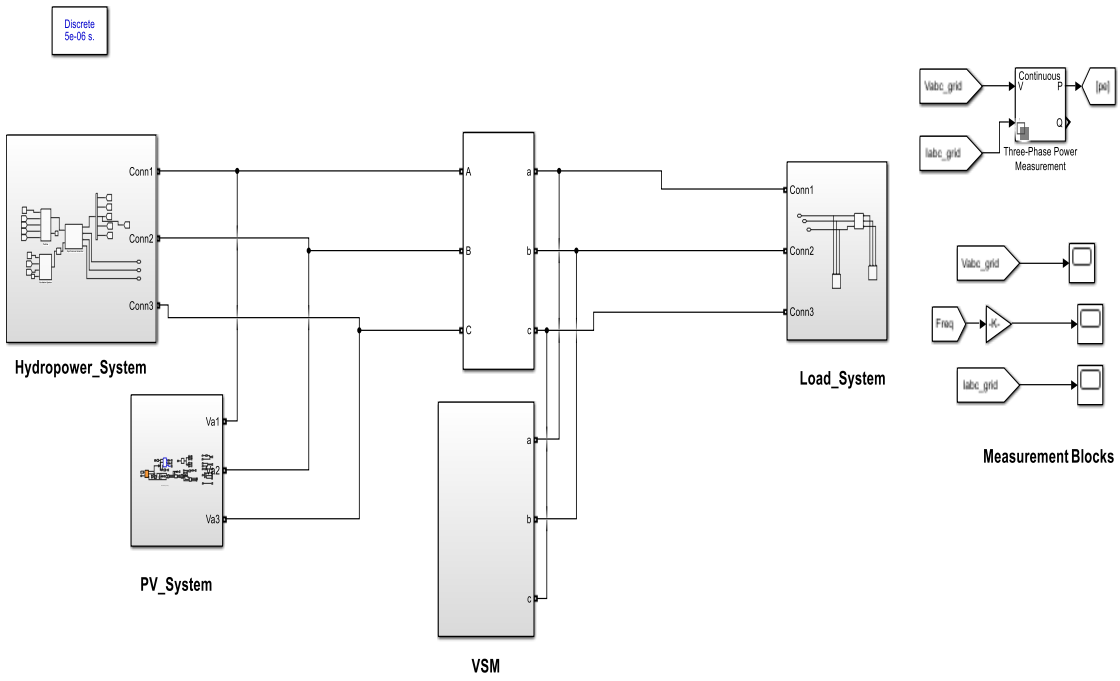

Figure 4.5 System during Case-II

Figure 4.6 shows the frequency of the grid after using VSM. When the additional load of 0.2 pu is switched on at t=3 seconds, the VSM comes into action because there is deviation in frequency by more than 2.5%. It is observed that after using VSM, the frequency of the grid during transient condition has been improved from 0.81 pu (40.5 Hz) to 0.93 pu (46.5 Hz). The deviation is about 7% from nominal frequency, which is within desirable limit (up to 15%) during transient condition. As the output frequency has been improved from 26% deviation to 10% deviation in paper (Adhikari, P. *et al.*, 2018). From the reference of this paper, the obtained frequency of the grid during transient condition in this thesis can be validated. The VSM has exchanged the power that is equivalent to the power which could have been provided by the real inertia of the system if it had been present there. After reaching to maximum deviation of 0.93 pu, the frequency recovers back towards normal value. During this, the VSM injects power to the grid and at about time t=14 seconds, the VSM is inactivated at the frequency comes about 0.975 pu (2.5% deviation of 1 pu). Then, the frequency comes back to normal range after few cycles.

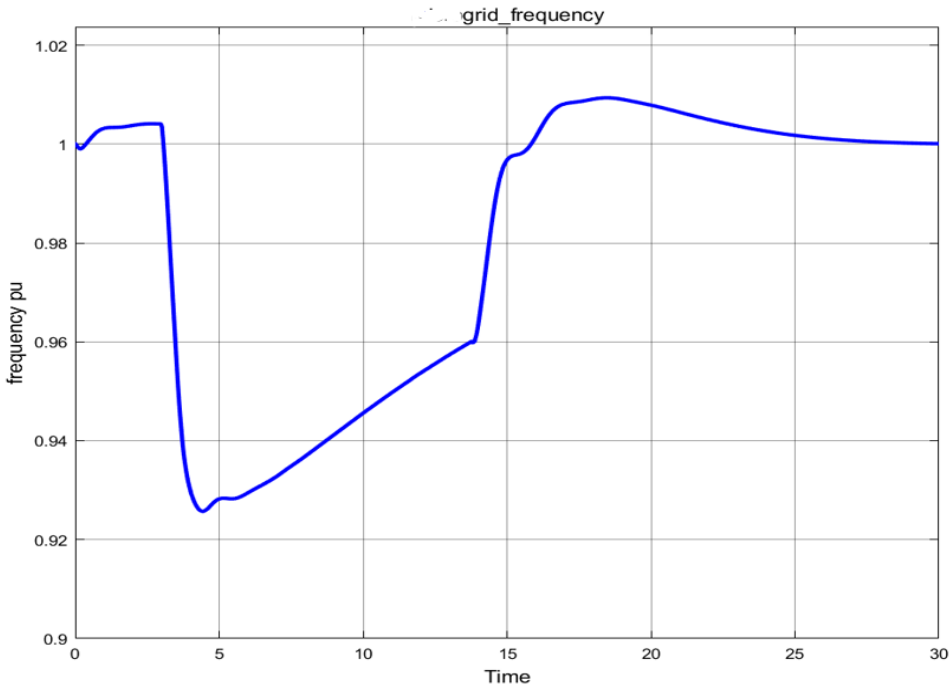

Figure 4.6 Frequency of the grid after using VSM

Figure 4.7 shows the magnified form of the grid voltage from time (3.10 to 3.18) seconds which shows that the voltage is of normal value and sinusoidal. The voltage of the grid is slightly reduced when the load is switched on at t=3 seconds but it is recovered after few cycles. When there is instant increase in load, the current will be increased on the same proportion instantly and the voltage drop increases. It will take some time to the excitation system to bring the voltage back to normal value.

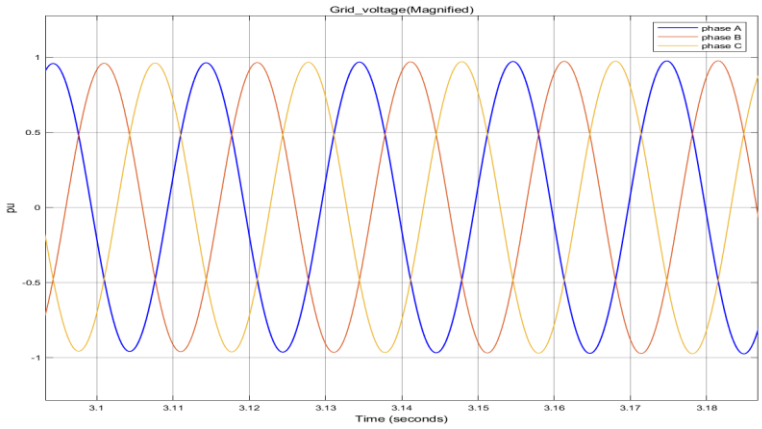

Figure 4.7 Voltage of the grid using VSM

Figure 4.8 shows the magnified form of grid current from time (7.95 to 8) seconds when the load is switched on at t=3 seconds. During this time VSM gives power thereby penetrating current until the frequency comes back to the steady state condition and the current is somehow distorted due to harmonics from the inverter. After filtering, the current is sinusoidal.

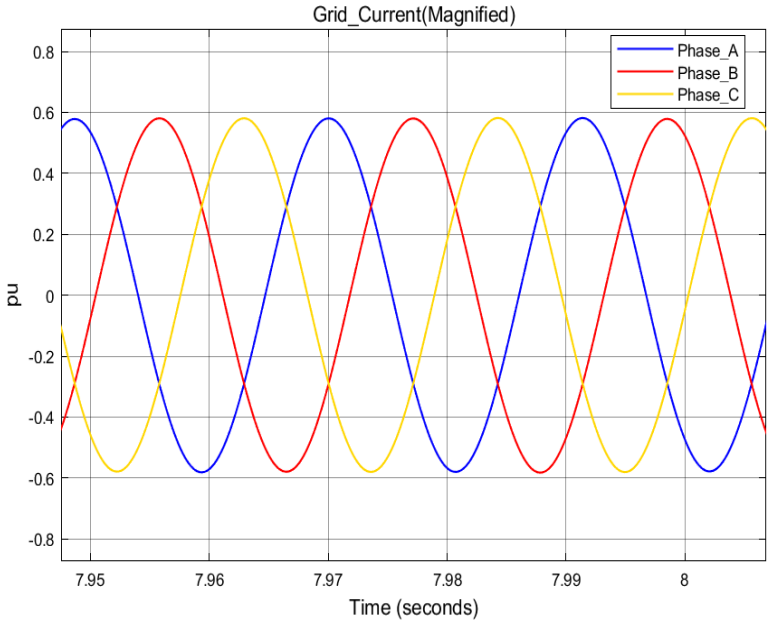

Figure 4.8 Current of the grid using VSM

Figure 4.9 shows the active power given by grid and the VSM. After three seconds, the VSM is activated when there is change in frequency by more than 2.5%, then the power given by VSM rises to about 0.1 pu and then it starts decreasing steadily. At about 8 seconds, the power by grid has reached to load power and it is supposed to be constant on that power but due the characteristics of the turbine, the power increases steadily and reached to about 0.61 pu up to 14 seconds. After 14 seconds, the grid power is equal to load power and becomes constant. The VSM power moves towards negative steadily after 8 seconds, which means it takes the extra power from the grid thereby charging its battery. Then, at about t=14 seconds, the frequency comes within 2.5% margin and the VSM goes into off state.

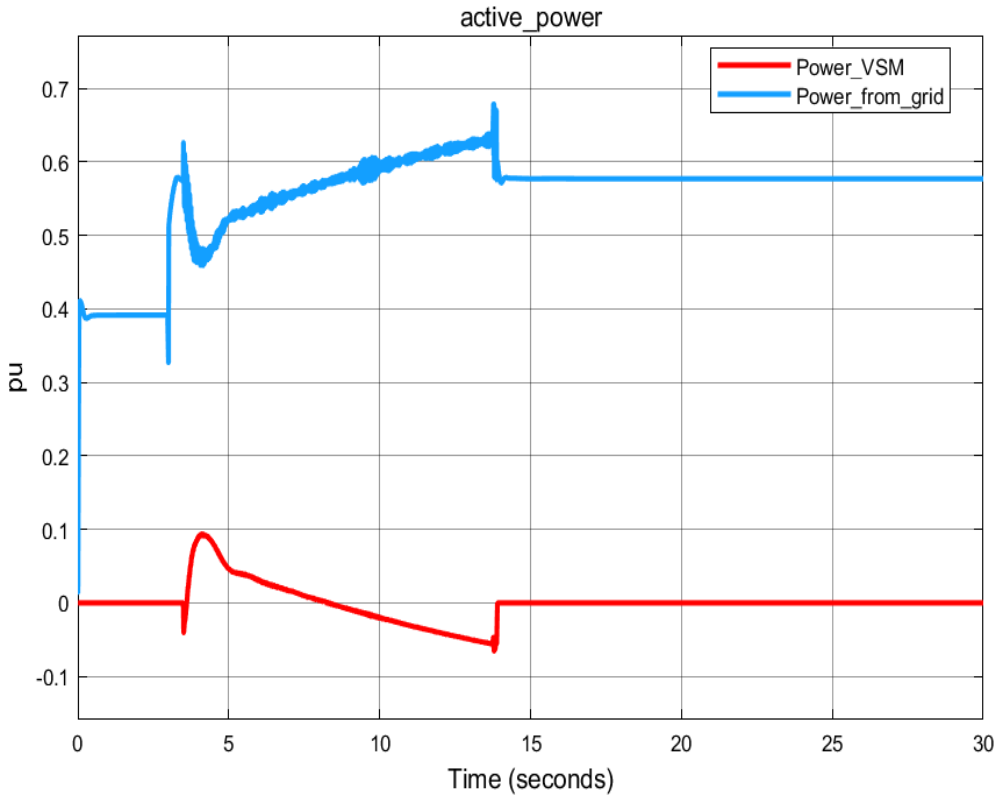

Figure 4.9 Power from the grid and VSM

CHAPTER FIVE: CONCLUSIONS AND RECOMMENDATIONS

5.1 Conclusions

Hydro system of 150 kVA has been designed and simulated in MATLAB. Along with this, a PV system of 10 kW has been added to make the total capacity of 160 kVA. A load of 0.4 pu has been switched on at all the time and 0.2 pu has been switched after 3 seconds of simulation starts. During transient condition, the frequency deviation has been observed by 19% which is beyond normal range as the maximum tolerable deviation is 15%. A VSM has been modelled and connected in the system, and the frequency deviation in the same load profile has been observed deviated by 7% which is within the normal range. Hence, from this thesis, it can be concluded that VSM can be employed to improve the transient stability of the system that lacks inertia, which might be due to increase in renewable energy penetration. With the implementation of VSM, the frequency deviation reduces from 19% to 7% and the transient stability has been increased. If there are large number of DGs or the inertia of the grid is poor, VSM of suitable rating can be implemented in the system to improve the transient stability of the system. Thus, VSM can be connected to the low-inertia system to increase its inertia thereby improving the transient stability.

5.2 Recommendations

1. This thesis consists of only active load. VSM can be employed in a system consisting of both active and reactive load.

2. Only PV and hydro system are connected to form the microgrid, more number of renewables sources of energy can be connected and VSM could be designed accordingly.

REFERENCES

Adhikari, P. *et al.*, 2018, 'Parallel operation of virtual synchronous machines with frequency droop control', *2017 7th International Conference on Power Systems, ICPS 2017*, pp. 116–120.

Bevrani, H., Ise, T. and Miura, Y., 2014, 'Virtual synchronous generators: A survey and new perspectives', *International Journal of Electrical Power and Energy Systems*, 54, pp. 244–254.

Bollen, M. *et al.*, 2009, 'Performance indicators for microgrids during grid-connected and island operation', *2009 IEEE Bucharest PowerTech: Innovative Ideas Toward the Electrical Grid of the Future*, pp. 1–6

Ceraolo, M. and Poli, D., 2014, 'Fundamentals of Electric Power Engineering: From Electromagnetics to Power Systems', *Fundamentals of Electric Power Engineering: From Electromagnetics to Power Systems*, 9781118679, pp. 1–532.

Cheema, K. M., 2020, 'A comprehensive review of virtual synchronous generator', *International Journal of Electrical Power and Energy Systems*, 120(February), p. 106006.

Damon, R. W., 2003, 'IEEE Standards', *IEEE Power Engineering Review*, PER-1(11), pp. 1–1.

Electronics, P., Circuit, E. and Simulation, O., 2004, 'Power electronics: electrical circuit-oriented simulation'.

Elsavad, M. A., Sarhan, A. G. M. and Abdin, A. A. M., 2017, 'Power angle control of virtual synchronous generator', *Journal of Electrical Engineering*, 17(2), p. 2.

Fitzgerald, A. E., Kingsley, C. and Umans, S. D., 2003, *Electric Machinery Fundamentals - 6th ed*.

Haji, D. and Genc, N., 2018, 'Fuzzy and PO Based MPPT Controllers under Different Conditions', *7th International IEEE Conference on Renewable Energy Research and Applications, ICRERA 2018*, 5, pp. 649–655

IEEE-SA-Standards-Board, 2014, *IEEE Guide for Selecting, Charging, Testing, and Evaluating Lead-Acid Batteries Used in Stand-Alone Photovoltaic (PV) Systems*, *Ieeexplore.Ieee.Org*.

Jun, L. and Dazhi, W., 2009, 'Study and simulation of a novel hysteresis current control strategy', *2009 2nd International Conference on Intelligent Computing Technology and Automation, ICICTA 2009*, 2, pp. 306–309.

Kollimalla, S. K. and Mishra, M. K., 2014, 'Variable perturbation size adaptive P&O MPPT algorithm for sudden changes in irradiance', *IEEE Transactions on Sustainable Energy*, 5(3), pp. 718–728.

Li, Q., Chen, J. and Jiang, D., 2020, 'Periodic variation in the effect of switching frequency on the harmonics of power electronic converters', *Chinese Journal of Electrical Engineering*, 6(3), pp. 35–45.

Liang, X. and Karim, C. A. Bin, 2016, 'Virtual synchronous machine method in renewable energy integration', *Asia-Pacific Power and Energy Engineering Conference, APPEEC*, 2016-Decem, pp. 364–368.

May, M. P. E. *et al.*, 2015, '2015 Index IEEE Power and Energy Magazine Vol. 13', *IEEE Power and Energy Magazine*, 13(6), pp. 1–1.

Meng, X., Liu, J. and Liu, Z., 2019, 'A Generalized Droop Control for Grid-Supporting Inverter Based on Comparison between Traditional Droop Control and Virtual Synchronous Generator Control', *IEEE Transactions on Power Electronics*, 34(6), pp. 5416–5438.

Mir, A. S. and Senroy, N., 2020, 'Self-Tuning Neural Predictive Control Scheme for

Ultrabattery to Emulate a Virtual Synchronous Machine in Autonomous Power Systems', *IEEE Transactions on Neural Networks and Learning Systems*, 31(1), pp. 136–147.

Phan, B. *et al.*, 2019, 'Transient Stability of Low Voltage Micro Grid', *Proceedings of 2019 International Conference on System Science and Engineering, ICSSE 2019*, pp. 169–173.

Pimprikar, T., Pawaskar, O. and Kumar, A., 2018, 'Virtual Synchronous Generator- A New Trend in Technology for Smart Grid Integration', *2018 International Conference on Information, Communication, Engineering and Technology, ICICET 2018*, pp. 1–5.

Sahay, K. B. and Yadav, A., 2018, 'Implementation of MPPT Technique in PV Array for a Varying Load by Modeling and Simulation', *iEECON 2018 - 6th International Electrical Engineering Congress*, pp. 1–4.

Sahu, P., Verma, D. and Nema, S., 2016, 'Physical Design and Modelling of Boost Converter systems', *2016 International Conference on Electrical Power and Energy Systems (ICEPES)*, pp. 10–15.

Sinha, S. *et al.*, 2018, 'DC DC Boost Converter for Thermoelectric Energy Harvesting', *Proceedings of the 2018 International Conference on Current Trends towards Converging Technologies, ICCTCT 2018*, pp. 1–4.

Song, F. F., Bi, T. S. and Yang, Q. X., 2005, 'Study on wide area measurement system based transient stability control for power system', *7th International Power Engineering Conference, IPEC2005*, 2005, pp. 1–4.

Tamrakar, U. *et al.*, 2015, 'Improving transient stability of photovoltaic-hydro microgrids using virtual synchronous machines', *2015 IEEE Eindhoven PowerTech, PowerTech 2015*.

Tamrakar, U. *et al.*, 2016, 'Current control techniques for applications in virtual synchronous machines', *2016 IEEE 6th International Conference on Power Systems,*

ICPS 2016.

Wang, B. *et al.*, 2018, 'Quantifying the synthetic inertia and load-damping effect of a converter-interfaced power source', *2018 IEEE International Energy Conference, ENERGYCON 2018*, pp. 1–6.

Yan, C. *et al.*, 2016, 'A comprehensive reliability assessment index system for regional grid with a large renewable energy penetration', *Asia-Pacific Power and Energy Engineering Conference, APPEEC*, 2016-Decem, pp. 619–622.

Yuan, C. *et al.*, 2016, 'Energy storage configuration strategy for virtual synchronous machine', *ECCE 2016 - IEEE Energy Conversion Congress and Exposition, Proceedings*, pp. 1–6.

Zhang, Y. *et al.*, 2019, 'Analysis of Inertia Mechanism of Grid-tied Photovoltaic Power Generation System with Virtual Inertia Control', *2019 4th IEEE Workshop on the Electronic Grid, eGRID 2019*.

Zhong, Q. C. and Hornik, T., 2012, *Control of Power Inverters in Renewable Energy and Smart Grid Integration*, *Control of Power Inverters in Renewable Energy and Smart Grid Integration*.

Zhu, Y., Wang, H. and Zhu, Z., 2021, 'Improved VSG control strategy based on the combined power generation system with hydrogen fuel cells and super capacitors', *Energy Reports*, 7, pp. 6820–6832.

PUBLICATION

Sah, S.k., and Shakya, S.R., 2022, ‘Enhancing the Transient Stability of PV-Hydro Microgrid using Virtual Synchronous Machine (VSM)’, *International Journal of Engineering Research and Technology*, 11(3), March (Paper accepted).

Shah_1

ORIGINALITY REPORT

13%
SIMILARITY INDEX

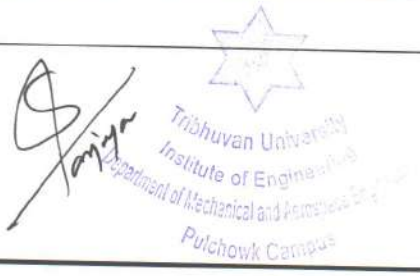

PRIMARY SOURCES

1	Prabin Adhikari, Suresh Prajapati, Indraman Tamrakar, Ujjwol Tamrakar, Reinaldo Tonkoski. "Parallel operation of virtual synchronous machines with frequency droop control", 2017 7th International Conference on Power Systems (ICPS), 2017 Crossref	78 words — 1%
2	www.elkraft.chalmers.se Internet	70 words — 1%
3	Ping Qian. "Study on Hysteresis Current Control and Its Applications in Power Electronics", Lecture Notes in Electrical Engineering, 2011 Crossref	50 words — 1%
4	documents.mx Internet	46 words — 1%
5	openprairie.sdstate.edu Internet	45 words — < 1%
6	hdl.handle.net Internet	41 words — < 1%
7	Ujjwol Tamrakar, David Galipeau, Reinaldo Tonkoski, Indraman Tamrakar. "Improving transient stability of photovoltaic-hydro microgrids using virtual synchronous machines", 2015 IEEE Eindhoven PowerTech, 2015 Crossref	37 words — < 1%